Acta Geologica Sinica (English Edition), 2022, 96(3): 875–890

Luku Alkali Syenite in the Hongge Ore District, SW China: Geochemistry, Geochronology and Metallogenic Significance

ZHOU Jiayun[1, 2, *], LIU Yingdong[1, 2], XU Li[1, 2], ZHU Zhimin[1, 2], GONG Daxing[1, 2] and JIANG Xiaoli[1, 2]

[1] *Technology Innovation Center of Rare Earth Resources Development and Utilization, Chinese Geological Survey, Chengdu 610041, China*
[2] *Institute of Multipurpose Utilization of Mineral Resources, Chinese Academy of Geological Sciences, Chengdu 610041, China*

Abstract: Luku alkali syenite is distributed throughout the southern end of the Hongge basic-ultrabasic intrusion in Panzhihua, Sichuan, SW China. Using LA-ICP-MS, the alkali syenite intrusion yielded a zircon U-Pb age of 264.5 ± 1.6 Ma, concordant with the ages of the E'meishan large igneous province (260 Ma). The intrusion displayed silica-saturated, Al-adequate and alkali-rich signatures, with SiO_2 62.07%–64.04%, Al_2O_3 16.26%–16.79% and $Na_2O + K_2O$ 9.17%–9.91% (averaging 9.31%). The rock falls into the alkaline zone on the SiO_2-A.R. diagram, as well as in the potassium zone on the K_2O-Na_2O diagram, indicating a potassium alkaline rock. The rock has a low total REE concentration and showed enrichment in LREE (LREE/HREE = 7.06–7.95), typical negative Eu anomalies (δEu = 0.73–0.80), trace element deficiencies in LILEs (Ba, K, Sr, Zr) and enrichment in HFSEs (Th, U, Nd, Sm, Ta and Nb), displaying crust and mantle element information. Zircons show a strong positive Ce anomaly and negative Eu anomaly, similar to the characteristics of crustal source magmatic zircon, however the $(Lu/Gd)_N$ ratio ranges from 1.48 to 3.17, and the $(Yb/Sm)_N$ ratio ranges from 38.49 to 77.15, which are similar to the characteristics of mantle-derived magmatic zircon. In the La/Yb-δEu correlation diagram, the data plots near the boundary between crust type and crust-mantle type. From the combined 'trinity' spatiotemporal relationship of Indosinian intermediate-acid alkali intrusive rocks in the Panxi area with E'meishan basalt and basic-ultrabasic intrusive rocks, the regional tectonic evolution and the partial melting model of the most intraplate magma sources, we believe that the Luku alkali syenite in Sichuan was formed from the partial melting of a crust-mantle source material, due to underplating of the mantle plume basic magma.

Key words: alkali syenite, mantle plume, LA-ICP-MS dating of zircon, REE mineralization, Hongge ore deposit

Citation: Zhou et al., 2022. Luku Alkali Syenite in the Hongge Ore District, SW China: Geochemistry, Geochronology and Metallogenic Significance. Acta Geologica Sinica (English Edition), 96(3): 875–890. DOI: 10.1111/1755-6724.14791

1 Introduction

The E'meishan large igneous province, formed by mantle activity around 260 Ma along the large, deep-seated, NS-trending fault in the Kangdian axis, mainly comprises continental flood basalt and associated layered basic-ultrabasic intrusive rocks and alkali syenite (Xu et al., 2001; Zhou et al., 2002). Among the aforementioned lithologies, the layered basic-ultrabasic intrusive rocks are renowned for their vanadium titano-magnetite. In-depth studies have been conducted on the rock's formation age and environment, petrology, petrogeochemistry, lithogenesis and the mineralization characteristics of this rock series, with fruitful results (Zhou, 2005; Zhong et al., 2007a). However, opinions still vary regarding the chronology and petrogenesis of the alkali syenite, which are closely spatially associated with basic-ultrabasic intrusive rocks (Luo et al., 2011). In terms of rock age, based upon the SHRIMP U-Pb dating of zircons from the Cida alkali intrusion which yielded an age of 225–221 Ma, younger than that of the Cida layered gabbro (256 Ma), Lin et al. (2006) believed that the alkali rocks and basic rocks are products of different stages of magmatic activity. On the other hand, according to the close association between alkali rocks and basic-ultrabasic rocks, the consistency of age and Sr-Nd isotopic characteristics between alkali rocks and gabbros, other researchers (Luo et al., 2006) believe that these rocks are cognate, contemporaneous and constitute a 'trinity' magmatic assemblage. The genesis of alkaline intrusions is still a matter of debate (Luo et al., 2011), some authors suggesting that alkali rocks were formed by fractional crystallization of basic magma (Zhong et al., 2007b). Recent studies have, however, revealed that the alkali rocks formed from the partial melting of crust, due to an underplating of basic magma (Xu and He, 2007; Shellnutt et al., 2008). There are a number of economic rare earth elements (REE), niobium (Nb) and tantalum (Ta) deposits, which are spatially and genetically associated with these alkali rocks by hydrothermal processes. The magmatic-metallogenic evolution of these alkali rocks, however, remains poorly understood.

* Corresponding author. E-mail: zhszjy@aliyun.com

To help clarify and resolve the controversy surrounding the genesis of the alkali syenite intrusion and to better define their relationship with the REE-Nb-Ta deposits, this paper provides geochemical analyses of the magmatic rocks, discussing sources and a genetic model for the alkali syenite. Plenty of new major and trace element, Sr-Nd-Pb isotope, zircon LA-ICP-MS chronology and zircon Hf isotope data of the intrusive rocks are presented, in order to elucidate the origin of the magmatism and the processes of mineralization.

2 Geological Setting

2.1 Regional geology

The Kangdian axis (KDA) is a significant part of the western margin of the Yangtze Platform. Its structural pattern, defined by NS-trending deep faults, is superimposed on a zone of late Proterozoic crustal extension (Fig.1a) (Munteanu et al., 2013). The geological architecture is the result of a complex tectonic evolution from Proterozoic lithospheric accretion, through the Paleozoic–Mesozoic continental margin, to a Cenozoic collision orogeny (Zhou et al., 2018). In particular, it formed the Panxi rift under extensional tectonic activity in the Hercynian–Indosinian period (Miao et al., 1986; Zhou et al., 2018) and the Jinpingshan Mountain under intracontinental convergence in the Yanshanian–Himalayan period, which is characterized by a double structure of earlier opening and later closing (Xu et al., 2007; Zhou et al., 2018), accompanied by extensive magmatism, sedimentary succession and terrane development.

The regional stratigraphy in the KDA can be divided into two tectonic units: the basement rocks and the overlying sedimentary rocks (Miao et al., 1986; Zhou et al., 2018). The basement consists of Archaean high-grade metamorphic rocks and Proterozoic meta-sedimentary rocks, with sedimentary Phanerozoic clastic and carbonate sequences (Hou Z Q et al., 2009; Zhou et al., 2018). Meanwhile, following the strong tectonic activity, the KDA underwent frequent magmatism. In particular, at 260 Ma, mantle plume-related magmatism produced the large-scale E'meishan basalt, basic-ultrabasic rocks and alkaline rocks, comprising the famous E'meishan igneous province in China.

These alkaline intrusions are located in the central-southern segment of the Panxi rift, occuring along the Anninghe fault belt and controlled by the Anninghe-Yimen fault and the Puxionghe-Puduhe fault (Zhang et al., 1988). These alkaline rocks are often ring-fracture intrusions, showing isolated dots or stock swarms, with an occurrence area of <1 km^2–32 km^2. These alkaline intrusions have two kinds of occurrence model, some being associated rock with basic-ultrabasic layered intrusions (Wang et al., 2013), while others are independent intrusions (Fig. 1a), such as Daping and Cida alkali rocks in Dechang, Maomaogou pienearite in Huili and Jijie alkali rock in Lufeng.

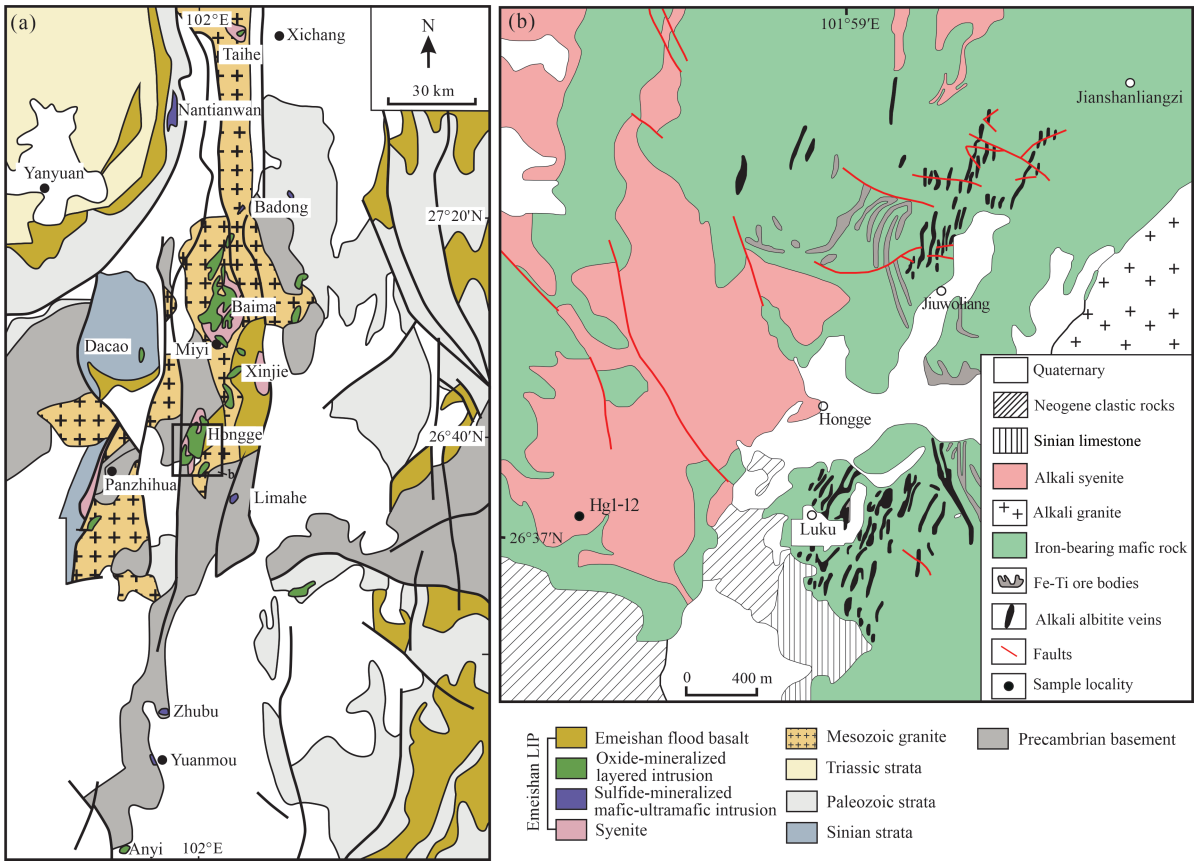

Fig. 1. (a) Distribution map of the Indosinian alkaline rock in the Panxi rift valley (after Zhou, 2013); (b) geological sketch of Luku REE, Nb and Ta deposits.

2.2 Ore deposit geology

The Luku alkaline rock is located at the southern margin of the Hongge ore district, Panzhihua, Sichuan Province, where the main phase of the associated stock is Fe-bearing basic-ultrabasic intrusions. There are about 159 relatively large alkaline veins, occurring in groups and distributed in belts, which intruded into basic-ultrabasic rocks. The rock types comprise alkali syenite, alkali syenitic pegmatite, alkali albitite and alkali granite (Fig. 1b). Among them, the alkali syenite and alkali granite are non-mineralized, however the alkali syenitic pegmatite and alkali albitite often have REE, Nb and Ta mineralization which display systematic increases in the alkalinity and intensity of mineralization, with progressive decreases in the rock's scale from NW to SE. About 42 ore (mineralized) veins have been discovered, mainly containing 16 kinds of REE minerals, including pyrochlore, allanite, laplandite, cebritholite, columbite-tantalite, johnstrupite, petersite and so on. REE, Nb and Ta mainly occur in pyrochlore, laplandite and allanite, which are dominated by La, Ce and Nd. The length of the orebody is generally 50–100 m and the thickness is 1–2 m, the scale of the deposit being medium.

However, the alkali syenite, which constitutes most rocks in the Hongge ore district, is a gray and massive structure with a hypidiomorphic granular texture. It is mainly made up of alkali feldspar, plagioclase and biotite with subordinate pyroxene and quartz, as well as accessory zircon and ilmenite (Fig. 2). The anhedral alkali feldspars (85 vol.%) are perthite (0.5–2 mm) with kasba and albite twins, the anhedral-heteromorphic plagioclase (5 vol.%, 0.8–3 mm) being both long and columnar. The subhedral-anhedral biotite (5 vol.%) is platy, the pyroxene being heteromorphic granular.

3 Sampling and Analytical Methods

3.1 Geochemistry and Sr, Nd and Pb isotopes

All samples for petrogeochemical analysis were collected from the Luku alkali syenite in the Hongge ore district, having been verified as being fresh, without typical weathering and alteration. The pit where they were sampled from is located at 26°37′3.29″N latitude and 101°58′28.43″E longitude. The samples for whole-rock major-element and trace-element analyses were washed and dried indoors, fresh parts being selected from the samples to be crushed to 200 mesh. The sample powders were then sent to the Institute of Multipurpose Utilization of Mineral Resources, Chinese Academy of Geological Science, for analysis. Major elements were analyzed using XRF, apart from FeO, which was measured by the potassium dichromate volumetric analysis method, with an error of <5%. Trace elements and REE analyses were conducted on a Thermo Xseries 2 type ICP-MS, with an error of trace elements <10% and an error of the REE analyses <5%. REE patterns and a primitive mantle-normalized trace element spider diagram were completed using the software Geokit (Lu, 2004).

The whole-rock Sr, Nd and Pb isotope analyses were completed by the Center of Mineral Resource Supervision and Testing at Central-South China. Analysis of Sr and Nd isotopes were performed on a Triton thermal-ionization mass spectrometer. Sample powders (200 mesh) were split into10 g quantities and placed in an oven at 80°C for 3 h, then dissolved by hydrofluoric acid and perchloric acid. Separation and purification of Sr was achieved by cation exchange resin. The Nd was separated and purified from the REE by cation exchange resin, after extraction by dilute hydrochloric acid. During the period of laboratory analysis, some international standard samples were adopted with which to monitor the instrument and analysis flow sheet. The $^{87}Sr/^{86}Sr$ and $^{143}Nd/^{144}Nd$ ratios are reported as normalized to the $^{86}Sr/^{88}Sr$ ratio of 0.1194 and the $^{146}Nd/^{144}Nd$ ratio of 0.7219, respectively. Analyses of NBS987 and GBW04411 yielded $^{87}Sr/^{86}Sr$ ratios of 0.71032 ± 0.00005 (1σ) and 0.76009 ± 0.00002 (1σ), which are identical, within the margin of error, to published values (0.71034 ± 0.00026 and 0.75999 ± 0.00020). Measurements of GBW04419 and the GSW Nd standard yielded a $^{146}Nd/^{144}Nd$ ratio of 0.512715 ± 9 and 0.512434 ± 8 (1σ), which are consistent with the standard values of 0.512725 ± 26 (2σ) and 0.512438 ± 6 (2σ), within the margin of error.

For Pb isotope determination, sample powders (200 mesh) were dissolved in Teflon vials with HF + HNO_3 and Pb was subsequently separated using anion-exchange

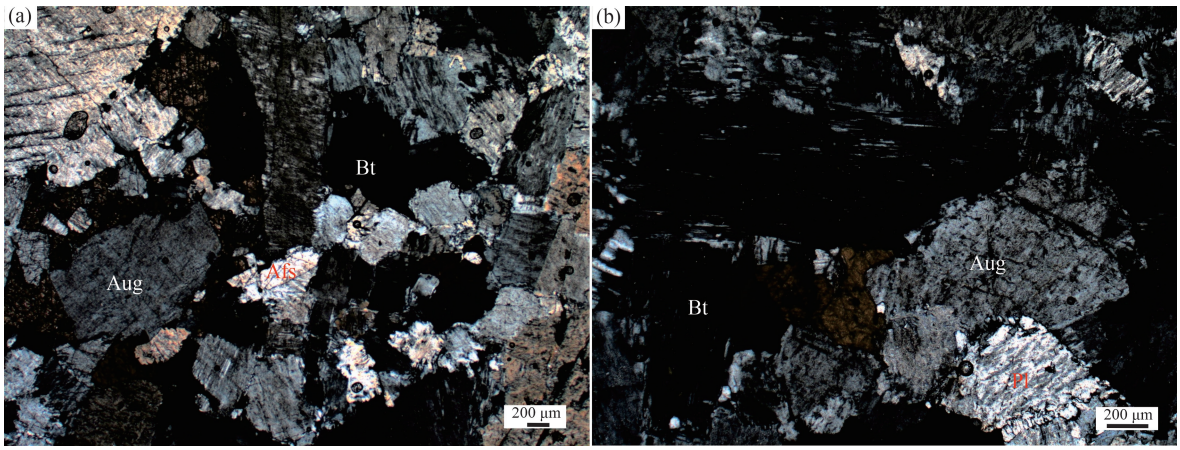

Fig. 2. Photomicrograph showing the texture of the Luku alkali syenite.
Aug–augite; Afs–alkali feldspar; Pl–plagioclase; Bt–biotite.

columns with diluted HBR as an eluent, following the procedure described by He et al. (2005). Pb isotope analysis was completed in a Neptune Plus. The $^{203}Ti/^{205}Ti$ ratio of 0.418652 was added as an internal standard to monitor and correct the fraction. Repeated analyses of the Pb isotope standard NBS981 yielded a $^{207}Pb/^{206}Pb$ ratio of 0.914826 ± 0.000007, a $^{208}Pb/^{204}Pb$ ratio of 36.7210 ± 0.0014, a $^{207}Pb/^{204}Pb$ ratio of 15.4984 ± 0.0005 and a $^{206}Pb/^{204}Pb$ ratio of 16.9414 ± 0.0005, consistent with the reference values of NBS981 (Li and Jiang, 2014; Xu et al., 2019): $^{207}Pb/^{206}Pb$ = 0.91464, $^{208}Pb/^{204}Pb$ = 36.722, $^{207}Pb/^{204}Pb$ = 15.4850 and $^{206}Pb/^{204}Pb$ = 16.9309.

3.2 Zircon U-Pb dating and Hf isotopic analyses

The samples (called DHG) for zircon LA-ICP-MS U-Pb dating, Hf isotope and trace element analysis were selected from the Luku alkali syenite in the Hongge ore district. Zircon grains were separated from alkali syenite samples using the conventional heavy liquid and magnetic techniques, followed by handpicking under a binocular microscope at the Langfang Geological Survey in Hebei Province, China. The individual crystals were mounted in epoxy resin, polished to reveal the cross-section of the grains, then photographed in both reflected and transmitted light, according to the method of Song (2002). After the grain interiors were exposed for cathodoluminescence (CL) and backscatter imaging, sites were selected for further analysis. The CL and BSE imaging, U-Pb dating, Hf isotope and trace element analyses of zircon were conducted at the MRL Key Laboratory of Metallogeny and Mineral Assessment, Institute of Mineral Resources, Chinese Academy of Geological Sciences, Beijing.

U-Pb isotopic and trace element analyses of zircon were simultaneously performed by a Newwave UP 213 laser-ablation system, coupled with a Bruker M90 MC-ICP-MS. The 213 nm ArF excimer laser, homogenized by a set of beam delivery groups, was focused on the zircon surface with an energy density of 2.5 J/cm^2. The ablation protocol employed a spot diameter of 25 μm at a 10 Hz repetition rate for at least 30 s. More detailed instrumental settings and analytical procedures were described by Hou K J et al. (2009). In the zircon U-Pb analysis, zircon GJ1 and Plešovice were used as the external standard for U-Pb dating and examined twice for every ten analyses, until 30 analytical points were completed. Off-line raw data selection, integration of background and analytical signals, as well as time-drift correction and quantitative calibration for U-Pb dating, were performed by ICP-MS Data 8.0 (Liu et al., 2008). Measured compositions were corrected for common Pb using non-radiogenic ^{204}Pb (Andersen, 2002). Concordia diagrams, binned frequency histograms and weighted mean ages were generated using Isoplot 3.0 (Ludwig, 2003), the results being reported with 1σ errors. For further data interpretation, the detailed analytical procedures and principles adopted were similar to those in Hou K J et al. (2009).

After the zircon U-Pb analyses, Hf isotope analysis was conducted on zircon grains in situ, using the Newwave UP213 laser-ablation system, attached to a Neptune MC-ICP-MS. A stationary spot, with a beam diameter of 55 μm and a repetition rate of 10 Hz, was used for the present analysis. In the analysis, helium was used as the carrier gas. Isobaric interference of ^{176}Lu on ^{176}Hf was corrected by measuring the intensity of the interference-free ^{175}Lu isotope and using a recommended $^{176}Lu/^{175}Lu$ ratio of 0.02655 (Dai et al., 2011) to calculate $^{176}Lu/^{177}Hf$ ratios. The isobaric interference of ^{176}Yb on ^{176}Hf was corrected by measuring the interference-free ^{172}Yb isotope and using a recommended $^{176}Yb/^{172}Yb$ ratio of 0.5886 (Dai et al., 2011) to calculate $^{176}Hf/^{177}Hf$ ratios. International standard GJ1 zircon samples were used for reference. The weighted average of $^{176}Hf/^{177}Hf$ of the GJ1 zircon samples was 0.282017 ± 0.000043 (n = 4, 2σ), consistent with the values (0.282015 ± 0.000019, using LA-ICP-MS) reported in the literature (Elhlou et al., 2006). Details of the instrumental conditions and test procedures were given in Hou et al. (2007).

Zircon trace element concentration results were simultaneously obtained during zircon U-Pb dating. Combined with external standard GJ1 and SRM, ^{29}Si was used as an internal standard to correct the trace element concentrations of the unknowns. A detailed calibration procedure for each element was presented in Wu et al. (2004). The average analytical error ranged from 15% to 5% for most trace elements, the relative standard deviation of minor trace elements with concentrations close to the limit of detection being up to 20%–40%.

4 Analytical Results

4.1 U-Pb dating of zircon

The external morphology of zircon, combined with its internal structure, has the ability to record magmatic evolutionary histories (Helena et al., 2014). Zircon grains from the Luku alkali syenite are euhedral, colorless and transparent, with columnar, granular shapes. They have a length of 100–120 μm, a width of 60–80 μm and a length/width ratio of 3:2. The crystal face remains intact and the crystal size is comparatively uniform. The study conducted by BSE and CL reveals that most grains are dark to slightly bright, thus revealing obvious oscillatory zoning, without inherited zircon cores, which indicate typical magmatic zircons (Fig. 3). A total of 30 analyses were conducted on 30 zircon crystals, which were separated from alkali syenite sample DHG, all spot analyses being performed in the magmatic zoning domains (Table 1), mostly agreeing with the apparent $^{206}Pb/^{238}U$ age of 247.19–274.16 Ma. However, seven data points were excluded, due to a relatively low analytical concordance in $^{206}Pb/^{238}U$ and $^{207}Pb/^{206}Pb$ ratios (Nos. 5, 9, 25, 28 points) or higher ages (Nos. 11, 15, 21 points), thus suggesting Pb mixing during the process of partial recrystallization or late thermal events. The other 23 analytical points with high U (440–955 ppm) and Th (562–1991 ppm) content and Th/U (0.73–2.29) ratio, yielded a concordia age (264.4 ± 1.4 Ma) within the margin of error (Fig. 4a). The $^{206}Pb/^{238}U$ age is 257.66–270.23 Ma with a weighted mean of 264.5 ± 1.6 Ma (MSWD = 1.9), which is interpreted as dating zircon crystallization to during the early Indosinian Period (Fig. 4b).

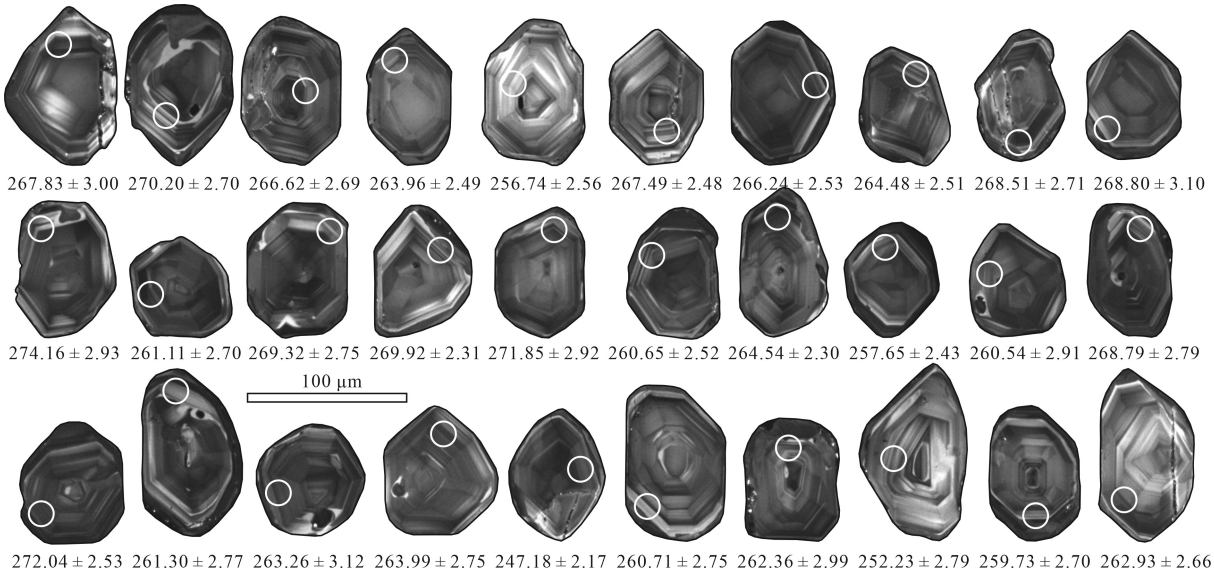

Fig. 3. CL images of zircon from the Luku alkali syenite.

Table 1 LA-ICP-MS U-Pb isotopic analytical data of zircon in Luku alkali syenite

No.	Pb*	Th	U	Th/U	Isotopic ratio						Apparent age (Ma)					
	(ppm)				$^{207}Pb/^{206}Pb$	1σ	$^{207}Pb/^{235}U$	1σ	$^{206}Pb/^{238}U$	1σ	$^{207}Pb/^{206}Pb$	1σ	$^{207}Pb/^{235}U$	1σ	$^{206}Pb/^{238}U$	1σ
1	149	713	440	1.62	0.0519	0.0011	0.3045	0.0066	0.0424	0.0005	279.69	46.29	269.87	5.16	267.84	3.01
2	182	845	537	1.57	0.0526	0.0011	0.3111	0.0064	0.0428	0.0004	322.28	48.14	275.02	4.97	270.23	2.70
3	162	766	507	1.51	0.0508	0.0011	0.2957	0.0060	0.0422	0.0004	227.85	43.51	263.06	4.70	266.62	2.69
4	180	843	629	1.34	0.0517	0.0010	0.2983	0.0058	0.0418	0.0004	333.39	44.44	265.06	4.57	263.97	2.49
5	344	1821	755	2.41	0.0546	0.0010	0.3057	0.0053	0.0406	0.0004	394.50	40.74	270.85	4.14	256.74	2.57
6	241	1166	586	1.99	0.0521	0.0011	0.3045	0.0064	0.0424	0.0004	287.10	52.77	269.92	4.99	267.49	2.49
7	261	1259	668	1.88	0.0526	0.0011	0.3056	0.0056	0.0422	0.0004	322.28	50.92	270.78	4.33	266.25	2.54
8	257	1279	627	2.04	0.0520	0.0009	0.3003	0.0053	0.0419	0.0004	283.40	40.74	266.62	4.17	264.49	2.52
9	168	758	561	1.35	0.0561	0.0022	0.3308	0.0142	0.0425	0.0004	457.45	85.17	290.15	10.83	268.51	2.72
10	344	1684	824	2.04	0.0532	0.0010	0.3118	0.0056	0.0426	0.0005	344.50	37.96	275.61	4.34	268.81	3.10
11	90	380	369	1.03	0.0513	0.0014	0.3064	0.0075	0.0434	0.0005	253.77	65.73	271.42	5.84	274.16	2.94
12	210	1027	576	1.78	0.0520	0.0010	0.2968	0.0060	0.0413	0.0004	287.10	44.44	263.94	4.70	261.12	2.70
13	173	701	955	0.73	0.0516	0.0009	0.3038	0.0057	0.0427	0.0004	333.39	38.89	269.39	4.44	269.32	2.75
14	217	1009	561	1.80	0.0524	0.0010	0.3093	0.0062	0.0428	0.0004	305.62	46.29	273.65	4.77	269.93	2.32
15	172	793	588	1.35	0.0509	0.0009	0.3020	0.0058	0.0431	0.0005	235.25	40.73	267.96	4.48	271.85	2.92
16	164	787	492	1.60	0.0524	0.0011	0.2986	0.0067	0.0413	0.0004	301.91	48.14	265.31	5.26	260.66	2.53
17	170	762	568	1.34	0.0510	0.0009	0.2948	0.0055	0.0419	0.0004	242.66	40.73	262.36	4.29	264.54	2.31
18	194	925	534	1.73	0.0529	0.0011	0.2973	0.0059	0.0408	0.0004	324.13	48.14	264.26	4.62	257.66	2.43
19	126	562	492	1.14	0.0516	0.0011	0.2932	0.0062	0.0412	0.0005	333.39	50.92	261.11	4.86	260.54	2.92
20	201	979	566	1.73	0.0512	0.0009	0.3007	0.0057	0.0426	0.0005	250.07	45.37	266.93	4.41	268.79	2.80
21	122	553	418	1.14	0.0532	0.0013	0.3163	0.0075	0.0431	0.0004	338.95	53.70	279.07	5.75	272.05	2.54
22	127	569	492	1.16	0.0522	0.0011	0.2982	0.0067	0.0414	0.0004	294.51	43.52	265.03	5.23	261.30	2.77
23	181	870	494	1.76	0.0519	0.0011	0.2973	0.0061	0.0417	0.0005	279.69	50.00	264.30	4.80	263.27	3.13
24	269	1342	673	1.99	0.0528	0.0010	0.3049	0.0066	0.0418	0.0004	320.43	42.59	270.23	5.14	263.99	2.75
25	309	1627	923	1.76	0.0561	0.0011	0.3027	0.0062	0.0391	0.0004	457.45	44.44	268.54	4.81	247.19	2.17
26	190	933	541	1.73	0.0520	0.0011	0.2960	0.0064	0.0413	0.0004	287.10	46.29	263.31	5.03	260.72	2.76
27	208	1011	538	1.88	0.0527	0.0011	0.3017	0.0063	0.0415	0.0005	316.73	15.74	267.73	4.92	262.37	3.00
28	190	919	518	1.77	0.0623	0.0014	0.3425	0.0075	0.0399	0.0005	683.35	48.15	299.07	5.65	252.24	2.79
29	398	1991	869	2.29	0.0518	0.0009	0.2936	0.0052	0.0411	0.0004	275.99	43.52	261.35	4.09	259.74	2.70
30	147	726	449	1.62	0.0526	0.0011	0.3022	0.0067	0.0416	0.0004	309.32	52.77	268.10	5.22	262.93	2.67

4.2 Lu-Hf isotopic characteristics of zircon

In situ Hf isotopic analyses of zircons from the Luku alkali syenite samples, along with the Hf zircon isotopic and calculation data results, are presented in Table 2. 23 spot analyses were obtained from 23 grains. In general, the $^{176}Lu/^{177}Hf$ ratios of magmatic domains are <0.002, with an average of 0.001648. The result indicates that time-integrated changes to the $^{176}Hf/^{177}Hf$ ratio as a result of the in situ decay of ^{176}Lu proceeded at virtually negligible rates (Kinny and Maas, 2003). Therefore, zircon effectively preserves the initial $^{176}Hf/^{177}Hf$ ratio, providing an enduring record of the Hf isotopic composition of its source environment at the time of crystallization. According to the average crystal components ($^{176}Lu/^{177}Hf$ = 0.008; Taylor and Melenan, 1985) and zircon U-Pb age to calculate the Hf isotopic model, $\varepsilon_{Hf}(t)$ values and T_{DM2}, the data show that the magmatic zircons from the Luku alkali syenite have stable Hf isotopic compositions, with initial $^{176}Hf/^{177}Hf$ ratios ranging from 0.282391 to 0.282565 and having an average value of 0.282465. The

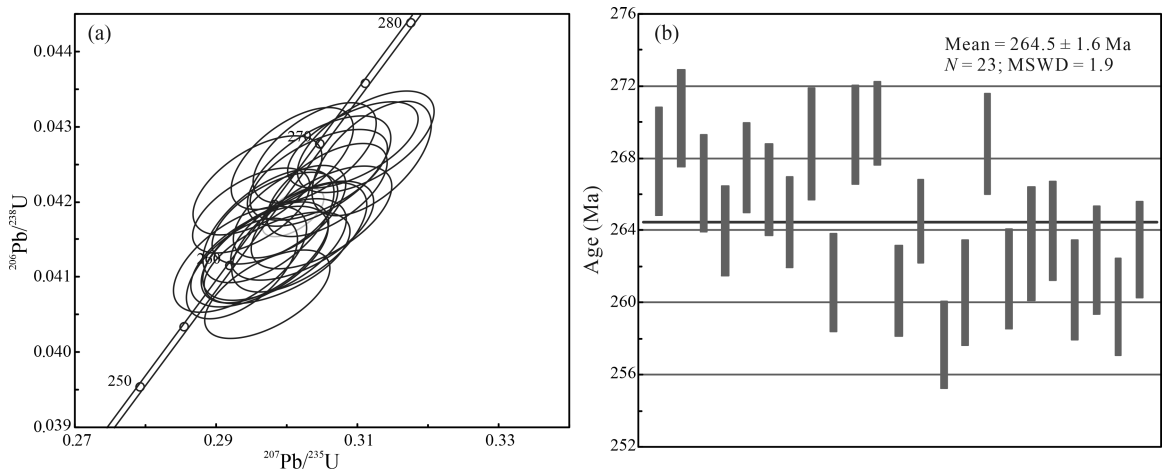

Fig. 4. Zircon U-Pb concordia diagram (a) and weighted average dating (b) of the Luku alkali syenite.

Table 2 Hf isotopic compositions of zircon in the Luku alkali syenite

No.	$^{176}Hf/^{177}Hf$	2σ	$^{176}Yb/^{177}Hf$	2σ	$^{176}Lu/^{177}Hf$	2σ	$\varepsilon_{Hf}(0)$	$\varepsilon_{Hf}(t)$	T_{DM1} (Ma)	T_{DM2} (Ma)	$f_{Lu/Hf}$
1	0.282495	0.000030	0.039803	0.000417	0.001366	0.000019	−9.78	−4.14	1080	1553	−0.96
2	0.282404	0.000030	0.046519	0.000833	0.001616	0.000014	−13.00	−7.36	1217	1759	−0.95
3	0.282493	0.000030	0.047804	0.000632	0.001583	0.000009	−9.86	−4.28	1089	1561	−0.95
4	0.282565	0.000036	0.051752	0.000842	0.001738	0.000013	−7.33	−1.83	991	1404	−0.95
6	0.282481	0.000029	0.057254	0.000400	0.001934	0.000016	−10.29	−4.76	1117	1592	−0.94
7	0.282496	0.000046	0.062914	0.000312	0.002036	0.000018	−9.76	−4.27	1099	1560	−0.93
8	0.282442	0.000042	0.047654	0.000870	0.001613	0.000009	−11.66	−6.13	1163	1677	−0.95
10	0.282408	0.000039	0.056269	0.000910	0.001900	0.000015	−12.86	−7.29	1221	1754	−0.94
12	0.282421	0.000040	0.044864	0.000310	0.001525	0.000006	−12.43	−6.96	1191	1727	−0.95
13	0.282497	0.000044	0.037228	0.000198	0.001274	0.000012	−9.74	−4.05	1076	1549	−0.96
14	0.282447	0.000045	0.054961	0.000613	0.001898	0.000011	−11.51	−5.92	1166	1667	−0.94
16	0.282453	0.000043	0.033464	0.000246	0.001135	0.000003	−11.27	−5.74	1132	1649	−0.97
17	0.282452	0.000049	0.064642	0.000443	0.002349	0.000025	−11.30	−5.90	1171	1662	−0.93
18	0.282517	0.000045	0.048376	0.000420	0.001708	0.000006	−9.00	−3.63	1058.	1513	−0.95
19	0.282445	0.000042	0.033711	0.000157	0.001200	0.000012	−11.56	−6.05	1146	1669	−0.96
20	0.282505	0.000032	0.027712	0.000544	0.000975	0.000026	−9.45	−3.72	1056	1528	−0.97
22	0.282444	0.000037	0.039185	0.000110	0.001333	0.000007	−11.62	−6.11	1152	1673	−0.96
23	0.282457	0.000048	0.053326	0.000612	0.001915	0.000036	−11.16	−5.71	1152	1649	−0.94
24	0.282484	0.000037	0.045428	0.000768	0.001509	0.000017	−10.19	−4.65	1100	1583	−0.95
26	0.282492	0.000041	0.046960	0.000685	0.001567	0.000011	−9.91	−4.45	1091	1568	−0.95
27	0.282463	0.000049	0.051444	0.000506	0.001743	0.000015	−10.94	−5.48	1138	1634	−0.95
29	0.282447	0.000045	0.075515	0.001304	0.002369	0.000024	−11.50	−6.20	1180	1677	−0.93
30	0.282391	0.000053	0.051788	0.000610	0.001611	0.000013	−13.48	−7.99	1236	1793	−0.95

negative Lu/Hf and $\varepsilon_{Hf}(t)$ ranges from −0.97 to −0.93 (average value of −0.95) and from −7.99 to −1.83 (the majority are negative, with an average of −5.33), indicating that the rock is mainly a product of the partial melting of crustal material (Griffin et al., 2004).

4.3 Trace element composition of zircon

Zircon trace element concentration results were simultaneously obtained during zircon U-Pb dating. The raw data calibrated by ICPMS Data 7.2 and associated calculations are listed in Table 3. The zircons measured in this study have variable concentrations of ΣREE, ranging from 550.89 to 1556.61 ppm. All trace element data show HREE-enriched REE patterns related to LREE, with stable and low ΣCe/ΣY ratios (0.03–0.25) and a marked left-sloping pattern of REE distributions. Moreover, the REE pattern zircons display pronounced positive Ce and negative Eu anomalies. In brief, the REE composition of the zircons show the characteristics of crustal magmatic zircon (Lei et al., 2013).

4.4 Whole-rock geochemistry

The analytical results of major and trace elements are presented in Table 4. The Luku alkali syenite has stable SiO_2 contents ranging from 62.07% to 64.04% and high $Na_2O + K_2O$ contents ranging from 9.17% to 9.91%, with an average of 9.31%. On the alkaline ratio (A.R.) vs. SiO_2 diagram (Fig. 5a), all samples plot in the alkaline field. On the Na_2O vs. K_2O diagram (Fig. 5b), the samples fall into the potassium alkaline series, which is obviously different from other independent alkaline rocks (such as Maomaogou) in the Indosinian Period (Luo et al., 2006). Besides, Luku alkali syenite has a high content of Al_2O_3 (16.26%–16.79%), AI (alkalinity index) > 0 and FSSI (feldspathoid silica-saturation index) > 0, showing them to be silica-saturated, Al-adequate and indicating a peraluminous quartz-bearing signature. The alkalinity index (AI) was defined as AI = Al − (K + Na) and the feldspathoid silica-saturation index (FSSI) was defined as FSSI = Q − [Lc + 2(Ne + Kp)]/100 (Frost and Frost, 2008).

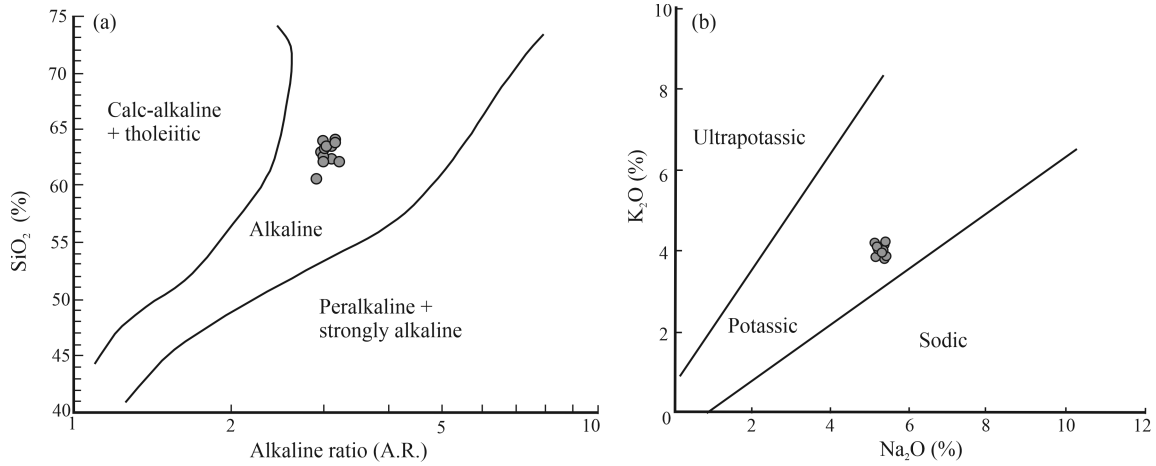

Fig. 5. (a) SiO_2-A.R. alkaline series discrimination graph of the Luku alkali syenite (after Wright, 1969); (b) K_2O-Na_2O diagram of the Luku alkali syenite (after Middlemost, 1975).

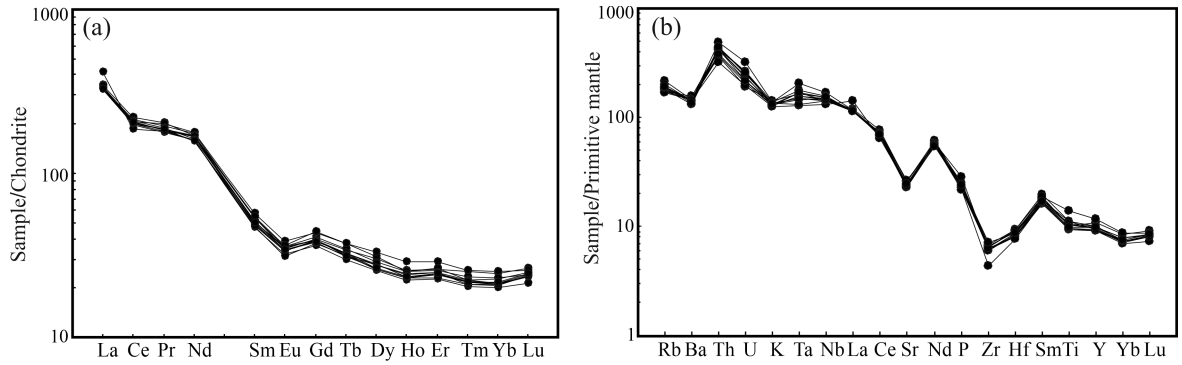

Fig. 6. Chondrite-normalized REE patterns (a, normalization values after Taylor and McLennan, 1985) and primitive mantle-normalized trace elements spidergrams (b, normalization values after Sun and McDonough, 1989) of the Luku alkali syenite.

Samples from alkali syenite have a high total REE content (ΣREE) ranging from 331.66 to 353.07ppm and some light REE enrichment (LREE/HREE = 10.33–12.23, La_N/Yb_N =13.67–16.74). On chondrite-normalized REE diagrams (Fig. 6a), they display a steeply right-sloping pattern, slight negative Ce (δCe = 0.63–0.81) and pronounced negative Eu anomalies (δEu = 0.73–0.80), which are similar to the REE distribution pattern characteristics of continental crust. On the primitive mantle-normalized multielement diagram (Fig. 6b), the samples display an obvious enrichment of high field strength elements (HFSEs such as Th, U, Nd, Sm, Ta and Nb) and depletion of large ion lithophile elements (LILEs such as Ba, K, Sr, and Zr), which simultaneously indicate signatures of both crust and mantle trace elements.

4.5 Whole-rock Sr-Nd-Pb isotopes

The whole-rock Sr and Nd isotope analysis results are given in Table 5. The Sr and Nd isotope ratios are calculated back to the formation time according to their zircon U-Pb data. The Luku alkali syenite shows high $(^{87}Sr/^{86}Sr)_i$ values, ranging from 0.705656 to 0.709938, but low $\varepsilon_{Nd}(t)$ values ranging from −4.8 to −1.5 (Fig. 7). Sr isotopes are negatively correlated with Nd isotopes and the samples are distributed along the direction of the mantle

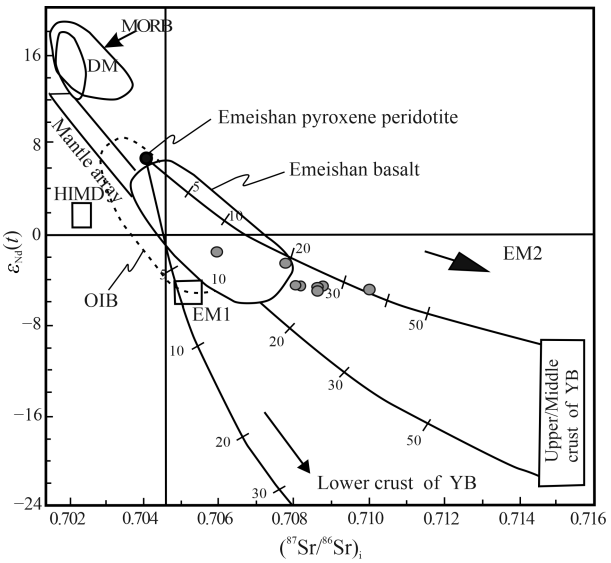

Fig. 7. The $(^{87}Sr/^{86}Sr)_i$ vs. $\varepsilon_{Nd}(t)$ diagram of the Luku alkali syenite in Panxi district.

Data sources: mantle array is after Zindler and Hart, 1986; OIB from Sun and McDonough, 1989; Yangtze upper/middle and lower crust from Chen and Jahn, 1998; Emeishan basalts and mafic intrusions from Xu, 2001 and Xiao, 2004.

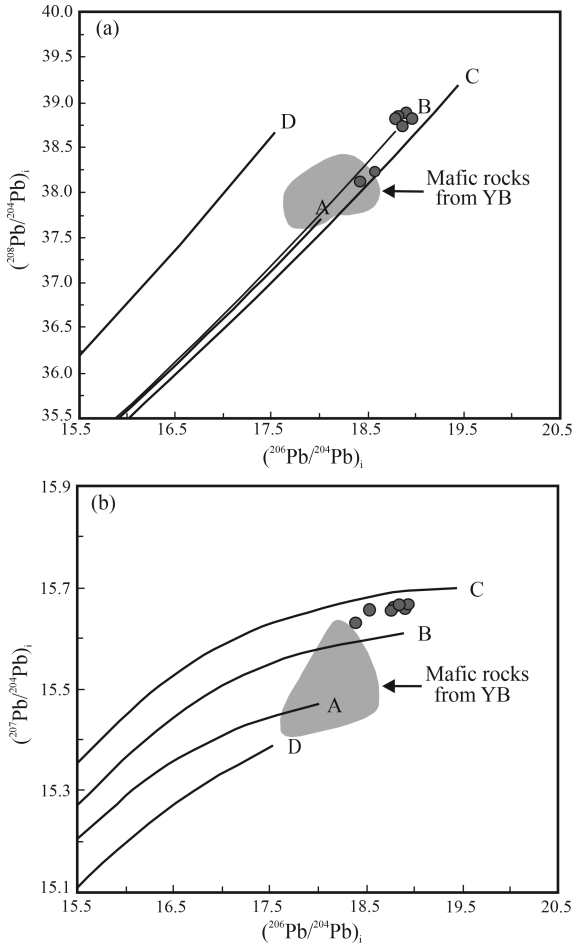

Fig. 8. Pb isotopic compositions for the Luku alkali syenite (mafic rocks from YB after Zhang et al., 2004).
A–mantle; B–orogen; C–upper crust; D–lower crust.

extending towards the upper crust.

Pb isotope analysis results are given in Table 6. The Luku alkali syenite shows high $^{206}Pb/^{204}Pb$ values of 18.9253 to 21.8619, $^{207}Pb/^{204}Pb$ values of 15.6607 to 15.8247 and $^{208}Pb/^{204}Pb$ values of 39.1487 to 40.76. The Pb isotope ratios are also calculated back to the formation time according to their zircon U-Pb data. Initial ratios are illustrated relative to other mantle reservoirs in Fig. 8, most samples lying between mantle and upper crust, indicating crustal material may have been involved in the generation of the plutons in significant proportions.

5 Discussion

5.1 Tectonic setting

Modern potassic igneous rocks occur in a wide range of tectonic environments, from continental to oceanic and intraplate settings, some of which are not apparently associated with subduction (Daniel and David, 2019). Potassic igneous rocks have been recognized throughout the world in five principal tectonic settings (Daniel and David, 2019). The HFSE (Ti, Y, Zr, Nb, Hf, Ta), REE, as well as the elements Th and P, are commonly assumed to be relatively immobile (Kaygusuz et al., 2018). Hence, they are normally considered to be most suitable for use in

Table 3 Trace element analysis (ppm) of zirocn from the Luku alkali syenite

No.	Ti	Nb	La	Ce	Pr	Nd	Sm	Eu	Gd	Tb	Dy	Ho	Er	Tm	Yb	Lu	Y	Hf	Ta	ΣREE	LREE/HREE	δEu	δCe
1	11.65	6.52	5.97	27.18	1.01	6.28	6.27	0.81	28.49	8.88	103.23	37.48	164.02	34.55	323.24	53.07	1080.77	6867.47	2.96	800.49	0.06	0.16	2.48
2	12.03	10.99	0.06	23.70	0.27	4.39	6.70	1.10	33.54	11.56	136.27	51.62	227.95	48.82	452.36	75.35	1505.16	6843.23	3.82	1073.68	0.03	0.18	24.81
3	9.76	7.87	0.26	21.02	0.27	3.56	5.63	0.73	26.85	8.48	97.09	34.88	151.61	33.42	312.61	51.57	1029.39	7815.16	3.49	747.98	0.04	0.15	17.47
4	12.95	16.68	0.06	33.58	0.38	5.71	8.54	1.23	45.06	16.01	197.82	74.76	337.01	71.31	658.91	106.22	2176.02	6952.39	4.95	1556.61	0.03	0.15	25.49
6	13.07	8.62	5.28	35.28	1.38	9.04	8.00	1.16	36.22	11.77	129.69	46.45	199.31	42.16	385.87	62.24	1323.48	6823.19	3.53	973.85	0.07	0.17	3.14
7	12.37	13.76	0.15	30.28	0.38	5.41	8.49	0.93	41.26	13.53	157.12	57.28	249.88	53.99	503.73	82.09	1668.61	7108.35	5.22	1204.53	0.04	0.12	21.28
8	14.55	10.33	0.42	28.06	0.47	5.72	8.01	1.09	37.17	12.30	142.10	51.52	226.11	47.79	447.52	70.73	1498.60	6929.42	4.11	1079.01	0.04	0.16	13.60
10	10.96	11.83	1.14	34.06	0.59	6.04	8.14	1.12	40.59	12.53	142.34	48.84	205.61	44.02	415.22	64.69	1389.00	7446.65	5.49	1024.92	0.05	0.15	10.14
12	14.33	9.13	0.05	21.89	0.33	4.58	6.94	0.79	30.28	10.45	121.24	43.75	187.81	40.91	379.53	62.21	1242.15	7336.36	4.36	910.76	0.04	0.14	19.63
13	5.68	7.39	0.01	28.54	0.15	2.02	3.01	0.55	15.48	4.86	56.99	21.46	98.41	23.70	246.70	49.02	641.92	9253.08	3.61	550.89	0.07	0.20	58.73
14	13.92	9.50	24.73	71.87	5.97	27.72	10.62	1.11	35.08	10.82	122.92	46.16	196.04	42.96	405.70	65.34	1302.83	7284.58	4.12	1067.04	0.15	0.16	1.40
16	12.56	7.82	0.04	19.48	0.25	3.94	6.04	0.91	29.48	9.66	112.70	42.79	191.06	41.02	383.34	63.61	1238.13	6977.73	3.27	904.30	0.04	0.17	22.91
17	10.91	13.43	0.06	27.76	0.47	6.87	11.06	1.38	47.82	15.45	181.92	67.19	288.56	63.11	578.80	94.36	1925.06	6851.30	4.56	1384.82	0.04	0.16	17.44
18	14.35	8.27	0.03	21.87	0.30	4.37	6.53	0.96	33.67	10.60	127.63	46.99	201.46	42.88	390.49	66.09	1316.67	6984.55	3.67	953.86	0.04	0.16	22.07
19	11.15	11.51	0.05	22.03	0.32	5.33	8.19	1.06	38.16	12.61	148.31	56.09	251.30	55.36	521.52	85.56	1632.35	7001.03	3.95	1205.87	0.03	0.15	20.00
20	10.55	7.45	0.04	20.56	0.27	3.72	5.85	0.74	27.95	8.64	99.71	35.48	151.01	33.15	298.11	49.43	1019.23	7285.58	4.28	734.64	0.04	0.15	22.71
22	14.52	12.08	61.78	132.60	12.39	49.78	13.35	1.47	38.39	12.17	137.39	53.62	240.67	51.80	481.19	80.54	1546.74	7022.46	4.63	1367.15	0.25	0.19	1.11
23	11.92	6.53	5.57	29.66	1.38	8.86	6.83	0.89	31.59	9.42	108.60	38.36	163.94	35.60	315.82	52.92	1112.67	7105.02	3.17	809.44	0.07	0.16	2.55
24	12.15	9.04	0.05	25.45	0.35	4.77	7.60	0.90	35.85	10.96	122.62	44.01	186.15	39.18	355.30	56.50	1226.75	7045.52	4.09	889.69	0.05	0.14	21.33
26	13.32	8.13	0.04	21.96	0.28	4.28	6.46	0.78	31.08	9.72	109.68	39.51	169.09	36.47	334.84	55.07	1106.44	7335.07	4.14	819.25	0.04	0.14	22.94
27	13.63	7.86	0.04	24.53	0.34	5.15	7.72	1.17	35.36	10.95	121.04	42.63	183.03	38.74	354.48	57.80	1219.14	6855.79	3.48	882.98	0.05	0.18	21.33
29	13.05	10.83	0.06	32.99	0.40	5.87	9.49	1.25	44.63	13.72	151.90	52.37	218.09	45.59	416.25	66.03	1467.91	6991.81	4.90	1058.64	0.05	0.15	24.24
30	13.32	6.91	10.68	38.55	2.11	13.44	12.09	1.55	48.83	14.44	160.73	55.80	236.69	51.06	465.30	76.13	1578.67	6881.02	3.07	1187.35	0.07	0.17	1.87

Table 4 Major (%), rare earth and trace element (ppm) compositions of the Luku alkali syenite

Sample	Hg1	Hg2	Hg3	Hg4	Hg5	Hg6	Hg7	Hg8	Hg9	Hg10	Hg11	Hg12
SiO_2	64.04	62.69	63.00	62.07	62.57	63.46	62.25	63.19	60.63	63.23	63.64	63.31
TiO_2	2.18	2.24	2.23	2.42	2.39	2.24	2.28	2.02	2.99	2.09	2.10	2.11
Al_2O_3	16.26	16.79	16.65	16.73	16.46	16.29	16.73	16.78	16.61	16.34	16.30	16.51
Fe_2O_3	2.50	4.23	4.55	4.69	4.18	3.69	4.79	4.10	4.74	3.66	3.56	3.69
FeO	2.36	0.97	0.80	0.70	1.09	1.28	0.55	0.94	1.35	1.33	1.26	1.32
MnO	0.069	0.068	0.073	0.082	0.078	0.062	0.073	0.060	0.085	0.077	0.068	0.071
MgO	0.68	0.74	0.72	0.72	0.75	0.72	0.78	0.67	0.90	0.74	0.67	0.72
CaO	1.71	1.85	1.80	1.68	1.92	1.78	1.81	1.70	2.09	1.77	1.70	1.78
Na_2O	5.12	5.38	5.30	5.40	5.22	5.42	5.33	5.36	5.38	5.16	5.19	5.31
K_2O	4.20	4.15	3.89	4.24	4.04	3.86	3.91	3.99	3.79	4.03	4.10	3.95
P_2O_5	0.21	0.20	0.22	0.21	0.20	0.20	0.21	0.19	0.25	0.20	0.19	0.21
I.O.	0.68	0.63	0.59	0.89	0.67	0.95	0.89	0.72	1.01	0.90	0.94	0.75
Total	100.01	99.94	99.82	99.83	99.57	99.95	99.60	99.72	99.83	99.53	99.72	99.73
A.R.	3.15	3.09	2.98	3.2	3.03	3.11	2.99	3.05	2.92	3.06	3.13	3.05
Na_2O+K_2O	9.32	9.53	9.91	9.64	9.26	9.28	9.24	9.35	9.17	9.19	9.29	9.26
AI	0.03	0.03	0.04	0.03	0.03	0.03	0.04	0.04	0.04	0.03	0.03	0.03
FSSI	0.76	0.72	0.75	0.72	0.74	0.75	0.74	0.74	0.72	0.76	0.76	0.75
La	79.3	78.6	81.3	79.0	77.1	79.6	78.6	80.3	97.7	80.6	77.3	77.3
Ce	130	125	135	127	123	126	129	121	114	127	122	124
Pr	18.5	17.6	19.3	19.0	17.6	17.3	18.0	16.9	17.2	17.4	17.2	17.7
Nd	81.9	78.8	79.3	83.3	77.9	73.8	76.0	74.6	79.4	77.7	75.0	74.0
Sm	8.26	7.82	8.18	8.67	7.69	7.50	7.75	7.17	8.40	7.40	7.31	7.60
Eu	2.01	1.97	2.08	2.22	2.07	1.96	2.04	1.85	2.10	1.94	1.81	1.99
Gd	8.13	7.94	8.45	8.97	7.99	8.02	8.00	7.46	9.06	7.95	7.73	7.82
Tb	1.27	1.22	1.30	1.40	1.19	1.20	1.22	1.12	1.40	1.22	1.18	1.17
Dy	7.66	6.98	7.39	7.92	6.98	6.63	7.17	6.54	8.39	6.69	6.65	6.71
Ho	1.45	1.38	1.42	1.43	1.37	1.30	1.32	1.27	1.64	1.32	1.30	1.33
Er	4.33	4.11	4.25	4.35	4.12	3.98	4.00	3.78	4.81	4.07	3.84	4.08
Tm	0.64	0.57	0.60	0.57	0.54	0.56	0.55	0.52	0.65	0.56	0.54	0.55
Yb	4.16	3.84	3.89	3.63	3.51	3.64	3.58	3.44	4.27	3.58	3.58	3.66
Lu	0.67	0.63	0.61	0.59	0.60	0.61	0.60	0.54	0.65	0.59	0.60	0.62
ΣREE	348.28	226.46	353.07	348.05	331.66	332.10	337.83	326.49	349.67	338.02	326.04	328.53
L/H	11.30	11.62	11.65	11.06	11.61	11.80	11.78	12.23	10.33	12.01	11.83	11.66
Eu/Eu*	0.74	0.76	0.76	0.76	0.80	0.77	0.79	0.77	0.73	0.77	0.73	0.78
Ce/Ce*	0.80	0.79	0.81	0.78	0.79	0.79	0.81	0.77	0.63	0.79	0.79	0.79
Cr	18.2	19.9	20.0	18.6	14.9	15.8	13.6	17.9	18.9	16.3	16.8	19.3
Ga	26.2	26.7	27.6	26.6	25.7	26.0	26.1	25.3	25.3	27.4	25.8	25.8
Rb	138	122	110	118	118	114	110	114	108	119	126	120
Sr	544	520	549	486	511	520	564	481	511	513	496	512
Y	49.0	44.5	45.0	45.6	43.0	43.6	45.3	41.2	53.5	42.0	42.6	44.7
Zr	72.2	69.2	73.6	76.0	71.9	68.8	71.1	69.8	67.3	71.1	49.2	79.4
Nb	121	111	101	110	100	104	107	105	94.2	100	104	108
Cs	1.67	0.79	0.66	0.73	0.83	0.57	0.51	0.72	0.81	0.81	0.82	0.75
Ba	1010	1010	1080	1020	990	982	1020	914	1020	1010	988	942
Hf	2.92	2.70	2.73	2.91	2.82	2.52	2.56	2.52	2.59	2.47	2.40	2.71
Ta	8.48	7.26	6.98	6.79	6.11	6.34	6.36	5.92	5.24	5.34	6.17	6.85
Th	41.5	36.4	35.8	30.5	36.0	35.4	31.5	35.4	27.4	32.4	37.2	37.9
U	6.67	5.47	4.54	4.01	4.86	5.03	4.30	5.53	4.13	4.56	5.24	5.39

A.R. = Al_2O_3 + CaO + (Na_2O + K_2O)/Al_2O_3 + CaO − (Na_2O + K_2O); A.I. = Al − (K + Na) (mol); FSSI = Q − [Lc + 2(Ne + Kp)]/100.

Table 5 Whole-rock Sr-Nd isotopic compositions of the Luku alkali syenite

Sample	$^{87}Rb/^{86}Sr$	$^{87}Sr/^{86}Sr$	I_{sr}	$^{147}Sm/^{144}Nd$	$^{143}Nd/^{144}Nd$	$\varepsilon_{Nd}(t)$
Hg1	0.734	0.71031 ± 0.00002	0.707547	0.0610	0.512516 ± 0.000005	−2.2
Hg2	0.679	0.70821 ± 0.00001	0.705656	0.0600	0.512479 ± 0.000005	−1.5
Hg5	0.668	0.71071 ± 0.00001	0.708195	0.0597	0.512180 ± 0.000006	−4.3
Hg6	0.635	0.71104 ± 0.00002	0.708652	0.0615	0.512186 ± 0.000004	−4.3
Hg7	0.564	0.71068 ± 0.00002	0.708556	0.0617	0.512177 ± 0.000005	−4.4
Hg8	0.686	0.71252 ± 0.00001	0.709938	0.0581	0.512163 ± 0.000003	−4.6
Hg9	0.610	0.71071 ± 0.00002	0.708408	0.0640	0.512165 ± 0.000004	−4.8
Hg10	0.670	0.71038 ± 0.00002	0.707854	0.0576	0.512182 ± 0.000007	−4.2

The ratio of $^{87}Rb/^{86}Sr$ and $^{147}Sm/^{144}Nd$ is calculated from the ICP-MS data of the samples, with I_{sr} and $\varepsilon_{Nd}(t)$ calculated to 264 Ma for all samples. The calculation parameters adopt $(^{147}Sm/^{144}Nd)_{CHUR}$ = 0.1967, $(^{143}Nd/^{144}Nd)_{CHUR}$ = 0.512638.

discrimination of the tectonic setting of potassic igneous rock (Daniel and David, 2019). In particular, Th, Ta and Hf are a group of refractory magmatophile elements, often entering into the magma in mantle partial melting, magma fractional crystallization and crust contamination processes, leading to content changing, however their ratio remains stable within a narrow range (Liu et al., 2005). The Luku alkaline syenite has a high Th content, ranging from 27.4 to 41.5 ppm, high Ta content, ranging from 5.24 to 8.48 ppm and a high Hf content, ranging from 2.40 to 2.92 ppm, with a relatively stable Th/Hf ratio (10.48–15.50), Ta/Hf ratio (2.02–2.90) and Th/Ta ratio (4.49–

Table 6 Whole-rock Pb isotopic compositions of the Luku alkali syenite

Sample	$^{206}Pb/^{204}Pb$	$^{207}Pb/^{204}Pb$	$^{208}Pb/^{204}Pb$	$^{238}U/^{204}Pb$	$^{232}Th/^{204}Pb$	$(^{206}Pb/^{204}Pb)_t$	$(^{207}Pb/^{204}Pb)_t$	$(^{208}Pb/^{204}Pb)_t$
Hg1	18.9253 ± 0.0004	15.6607 ± 0.0004	39.1487 ± 0.0012	0.19	1.19	18.409	15.634	38.105
Hg2	21.8619 ± 0.0006	15.8247 ± 0.0004	40.7630 ± 0.0010	0.20	1.34	21.285	15.795	39.515
Hg5	19.4400 ± 0.0005	15.7002 ± 0.0005	39.9489 ± 0.0014	0.17	1.26	18.973	15.676	38.825
Hg6	19.2925 ± 0.0004	15.6995 ± 0.0005	39.7212 ± 0.0016	0.15	1.08	18.874	15.678	38.765
Hg7	19.1894 ± 0.0005	15.6863 ± 0.0005	39.7912 ± 0.0010	0.14	1.06	18.794	15.666	38.849
Hg8	19.0755 ± 0.0006	15.6871 ± 0.0006	39.2354 ± 0.0017	0.18	1.17	18.581	15.662	38.207
Hg9	19.0877 ± 0.0008	15.6792 ± 0.0007	39.4832 ± 0.0025	0.10	0.69	18.806	15.665	38.875
Hg10	19.4018 ± 0.0004	15.7005 ± 0.0003	40.0250 ± 0.0008	0.18	1.29	18.902	15.675	38.871

The ratio of $^{238}U/^{204}Pb$ and $^{232}Th/^{204}Pb$ is calculated from the ICP-MS data and Pb isotope ratio of the samples, initial isotope ratios being calculated according to the Pb isotope single-stage evolution model, t = 264 Ma being used in the calculation.

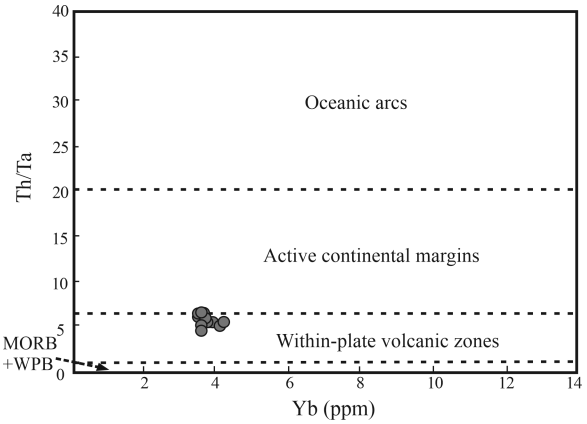

Fig. 9. The tectonic background for the Th/Ta-Yb diagram of the Luku alkali syenite (after Goton and Schandl, 2000).

6.07). On Th/Ta vs. Yb discrimination diagrams for potassic igneous rocks (Fig. 9), all samples plot in the intraplate field.

The Panxi area is a tectonic-magma province which is located along the western margin of the Yangtze platform. Its current geological structural pattern is the product of a series of geotectonic events, having mainly undergone extension and compression of continental crust associated with widespread magmatism (Munteanu et al., 2013). At ca. 260 Ma, mantle plume-related magmatism in the Panxi region generated the E'meishan flood basalts, along with ultramafic and silicic volcanic rocks and numerous intrusive bodies (peridotites, pyroxenites, layered gabbros, syenites, granites) (Munteanu et al., 2013), so that the tectonic setting of the alkaline intrusions should be consistent with that of the simultaneous E'meishan basalt and mafic-ultramafic intrusions (Zhong et al., 2007a). The intraplate character of the E'meishan magmatism is generally accepted (Munteanu et al., 2013). Thus, the intraplate continental extension environment of the Luku alkali syenite is consistent with the regional tectonic setting's evolution.

5.2 Source of the syenite

Alkaline rocks can originate from the mantle (Gomes et al., 2011), during the evolution of crustal magma chambers at different depths (Andrea et al., 2015) and from mixting of crustal and mantle material (Zhou et al., 1996). In particular, it is widely accepted that sodic alkaline rocks originate from mantle source. However, there are different views on the source of potassic alkaline rocks: (1) low degree partial melting of mantle lithosphere containing phlogopite and/or potash amphibole (Foley, 1992); (2) partial melting of a mantle wedge modified by subducted sediment and fluid derived from dehydration of a subducted slab, which is enriched in K and other alkali metals (Sokól et al., 2018).

The Luku alkali syenite intrusion yielded a zircon U-Pb age of 264.5 ± 1.6 Ma, 5 Ma earlier than the zircon U-Pb age of Li et al. (2017) (258 Ma), although concordant with the ~260 Ma ages of the E'meishan large igneous province (Wang et al., 2013; Zhou et al., 2013). Indosinian alkali intrusive rocks are spatially associated with the E'meishan basalt and basic-ultrabasic intrusive rocks in the Panxi area, named a 'trinity' spatiotemporal relationship (Luo et al., 2006), so they should be the product of the same magmatic activity.

It has been generally accepted that magma in the ~260 Ma E'meishan large igneous province was produced in the intraplate environment (Munteanu et al., 2013) and the geochemical characteristics of the Luku alkaline rocks also show a significant continental extension environment. As such, it is not possible that the Luku alkali syenite originated from partial melting of the mantle wedge modified by fluid in the subduction zone. In addition, contemporaneous alkaline and gabbroic intrusions are commonly observed around basalt in the inner zone of the ~260 Ma E'meishan large igneous province, the distribution, age and geochemistry of these igneous rocks, especially the whole rock Sr-Nd isotopes and zircon Hf isotopes for syenite and hornblende gabbro, indicate that the mantle source plays a major role in the formation of magma (Zhong et al., 2007b; Zhang et al., 2019). But in this study the detailed petrology, chronology, major and trace element geochemistry, especially whole rock Pb-Sr-Nd isotopes and zircon Hf isotopes for the Luku alkali syenite from Hongge ore district, southern Panxi rift, indicate a significant contribution from both crustal and mantle material.

On a chondrite-normalized REE diagram (Fig. 6a) and a primitive mantle-normalized multielement diagram (Fig. 6b), Luku alkali syenite displays obvious enrichment of Th and U, along with depletion of Ti, which is similar to crustal values. In contrast, the enrichment of Nb and depletion of Ba, K and Zr indicates that the magmas were predominantly from a mantle-derived component (Rudnick and Gao, 2003). The ratio of strongly incompatible elements in magmatic rocks, as it is unaffected by the fractionation process, can be used to

directly discuss magma source properties such as isotopic ratio (Zhang et al., 2005). For example, HFSEs Nb and Ta have similar ionic radii and show consistent behaviors during magmatic evolution. In most magmatic processes, the ratio of Nb/Ta varies over a very narrow range (Luo et al., 2006). Mantle and chondrite have a concordant Nb/Ta ratio (~17.5 ± 2.0; Weyer et al., 2002), while the crust has an Nb/Ta ratio of 11–12 (Green, 1995), showing a significant difference. Thus, the ratio of Nb/Ta is an effective parameter for discriminating mantle-derived rocks from crust-derived rocks (Luo et al., 2006). The Luku alkali syenite shows strong enrichment in Nb and Ta, with concentrations of 94.2–121 ppm and 5.24–8.48 ppm respectively, Nb/Ta ranging from 14.27 to 18.73 and averaging 16.41. In the La/Yb-δEu correlation diagram (Fig. 10), data plots mainly within the crust type field and near the boundary between crust type and crust-mantle type. Thus, the Luku alkali syenite was possibly sourced from the crust-mantle source area (Zhang et al., 2014).

Generally, $^{87}Sr/^{86}Sr > 0.710$ is considered as indicating crust-derived material, with $^{87}Sr/^{86}Sr < 0.705$ indicating mantle-derived material (Ni et al., 1999). The Luku alkali syenite shows high $(^{87}Sr/^{86}Sr)_i$ values, ranging from 0.705656 to 0.709938, indicating that a mantle-crustal origin is likely. Generally, the $^{207}Pb/^{204}Pb$ values would increase, in turn, from lower crust, mantle to upper crust, so the $^{207}Pb/^{204}Pb$ values can be used as a basic variable to trace the magma source. In this study, the Luku alkali syenite shows high $^{207}Pb/^{204}Pb$ values of 15.6607 to 15.8247, samples plotting mainly between the crustal extended line and the mantle extended line (Fig. 8a), indicating that they are derived from the crust-mantle source area. The $\varepsilon_{Nd}(t) = -1.5$–$-4.8$ indicate that they are derived from crustal materials, or at least have been significantly contaminated with crustal materials during their formation.

Different trace element profiles of zircons qualitatively reflect the evolution and chemical variation of their parent magma. Zircon crystals contain a record of multiple geological events (Li H et al., 2014) and thus zircon studies play an important role in distinguishing the origin of igneous rocks (Nardi et al., 2012). Previous studies pointed out the significantly different REE patterns between mantle zircons and crustal zircons. Zircons with a mantle affinity have positive Ce anomalies, slightly negative or no significant Eu anomalies and a flat pattern of HREE distributions, with $(Lu/Gd)_N$ varying from 1 to 10 and a $(Yb/Sm)_N$ of 3–30 (Belousova et al., 1998). In contrast, zircons with a crustal affinity always have pronounced positive Ce anomalies, negative Eu anomalies (Ce-enriched yet Eu-depleted REE patterns) and $(Yb/Sm)_N > 100$ (Belousova et al., 1998; Hoskin et al., 2000; Li et al., 2000). In this study, the most magmatic zircons are considered to have positive Ce and negative Eu anomalies, thus indicating their crust-derived magmatic origin. Simultaneously, the zircons have a $(Lu/Gd)_N$ ranging from 1.48 to 3.17 and a $(Yb/Sm)_N$ ranging from 38.49 to 77.15, similar to the characteristics of mantle-derived magmatic zircons.

The zircon Lu-Hf isotope analysis is also an important method for tracing the geochemical origin of rocks. In the study of Hf isotopes, the Hf isotopic composition of some important geochemical reservoirs is the basis for discussion. The presence of such enriched (low Lu/Hf) reservoirs in the lower crust was demonstrated by the highly negative $\varepsilon_{Hf}(t)$ values of −12 and −10, as well as the extremely low $^{176}Hf/^{177}Hf$ ratios (<0.282772) (Kinny et al., 2003). Depleted (high Lu/Hf) mantle was a detected source for magmatic rocks, so that rocks yielded $\varepsilon_{Hf}(t)$ values up to +14 (present-day oceanic basalts have $\varepsilon_{Hf}(t)$ up to +23) and high $^{176}Hf/^{177}Hf$ ratios (>0.282772) (Kinny et al., 2003). Studies on zircon Hf isotopes of the Luku alkali syenite found that the $\varepsilon_{Hf}(t)$ values vary from −7.99 to −1.83, with an average of −5.33, significantly different from that of depleted mantle, showing lower crust characteristics. In the zircon T-$\varepsilon_{Hf}(t)$ diagram, the data predominantly plot in the lower crust source field (Fig. 11). The $^{177}Hf/^{176}Hf$ values of zircons sampled from Luku alkali syenite vary at 0.282391–0.282574, with an average value of 0.282465, which significantly deviates from the $^{177}Hf/^{176}Hf$ values of depleted mantle (0.2831–0.2835), EM1 enriched mantle (0.2826–0.2827) and EM2 enriched mantle (0.2828) (Zindler et al., 1986), but is close to those of the lower crust (<0.282772) (Kinny et al., 2003). Therefore, the overall characteristics of the zircons indicate that the host rocks were derived from ancient crust.

In fact, some researchers that believed that these alkaline magmas originated from crystal fractionation of mantle basic magma, have also noticed the crustal

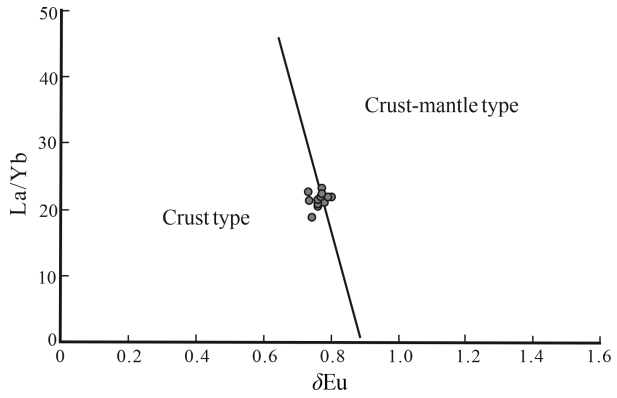

Fig. 10. (La/Yb)−δEu diagram of the alkali syenite from Luku (after Zhang et al., 2014).

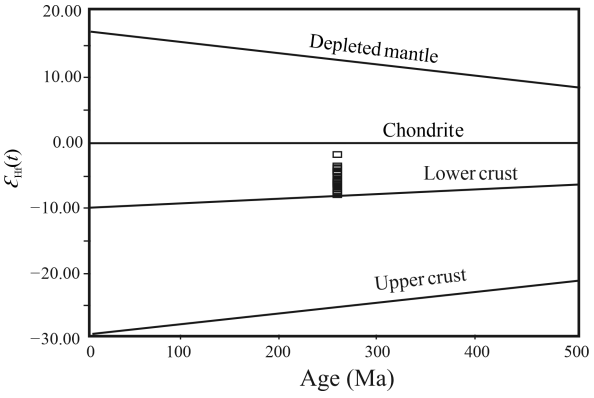

Fig. 11. Zircon age−$\varepsilon_{Hf}(t)$ diagram of the Luku alkali syenite (modified from Griffin et al., 2002).

information of alkaline magmas, interpreting them as crustal contaminants (Zhong et al., 2007b). Generally, the magmatic rocks, contaminated by the crust, are characterized by showing a high primitive mantle-normalized Th/Nb ratio (>>1) and a low Nb/La ratio (<1), with pronounced negative Nb, Ta, Ti anomalies on the primitive mantle-normalized multielement diagram (Kieffer et al., 2004). However, according to studies of trace elements, the Luku alkali syenite has a low Th/Nb ratio (0.29–0.36) and a high Nb/La ratio (0.96–1.53, average 1.32), without the pronounced negative Nb, Ta, Ti anomalies on the primitive mantle-normalized multielement diagram, which indicates that the geochemical compositions of the alkali rocks reflect insignificant crustal contamination.

Above all, whole rock major and trace element geochemistry, Sr-Nd-Pb isotopes, zircon trace elements and Lu-Hf isotopes for Luku alkali syenite, simultaneously display crust and mantle characteristics, indicating significant contributions from crustal and mantle material. The combination of the 'trinity' spatiotemporal relationship of Indosinian intermediate-acid alkali intrusive rocks in the Panxi area, with E'meishan basalt and basic-ultrabasic intrusive rocks, indicates that the Luku alkali syenite was formed from the partial melting of a crust-mantle source.

5.3 Petrogenesis

The E'meishan large igneous province (ELIP) in SW China is thought to be one of the best examples of the world's large igneous provinces with a good outcrop (Wang et al., 2013). In the inner zone of the ELIP, the alkaline syenite (260 Ma) is spatially associated with basalts, gabbroic and felsic intrusions, being commonly observed around basalts in the Panxi rift (Zhang et al., 2019), which implies that they have a close relationship in their origins. The intraplate environment of the magmatism is generally accepted. However, there are currently two views on magma generation and emplacement: back-arc extension caused by subduction and mantle plume (Munteanu et al., 2013). Based on the simultaneity of the E'meishan magmatism and the subduction of the Paleotethys oceanic crust at the western margin (present position) of the Yangtze craton, some authors believe that the E'meishan magmatism is related to a crustal extension behind the subduction (Munteanu et al., 2013), but this cannot explain the occurrence of the elevated PGE contents in many mafic-ultramafic intrusions from the Panxi region and in some E'meishan basalts (Munteanu et al., 2011). In the past two decades, the mantle plume model of the E'meishan large igneous province has met general approval (Xu and He, 2007). In fact, the mantle plume and rift models are not incompatible. A combination of the back-arc and plume models was proposed by Xiao et al. (2008), who inferred the presence of a mantle plume causing the Late Devonian rifting of the Changdu-Simao block from the Yangtze craton, with the opening of the Jinshajiang River and the subsequently induced eruption of the E'meishan basalts.

Currently, two models have been proposed for the origin of these Indosinian alkaline intrusions in the Panxi area (Luo et al., 2011), including the following: (1) fractional crystallization of basic magma (Zhong et al., 2007b); (2) partial melting of the crust, due to basic magma underplating (Xu and He, 2007; Shellnutt et al., 2008). Firstly, a study by Astis et al. (2000) showed that the continental crust provides potassium in the genesis of potassium magma. The currently accepted view is that potassium-rich volcanic rocks cannot be produced by partial melting of mantle peridotite and crustal materials must be involved in the diagenetic process (Muller et al., 2001). Secondly, it is difficult to explain that the Luku alkali syenite simultaneously indicates signatures of crustal material and mantle material through fractional crystallization of basic magma under a low degree of crustal contamination. Thirdly, the layered basic-ultrabasic rocks, spatially associating with the Luku alkali syenite in the Hongge ore district, display a slight enrichment of LREE, a flat REE pattern showing no obvious Eu anomaly (Hu et al., 2001). But samples from alkali syenite have some LREE enrichment (LREE/HREE = 10.33–12.23, La_N/Yb_N = 13.67–16.74). The chondrite-normalized REE diagram (Fig. 6a), displays a steeply right-sloping pattern and pronounced negative Eu anomalies (δEu = 0.73–0.80), distinct from the REE distribution pattern characteristics of basic-ultrabasic rocks. Furthermore, the Hongge layered basic-ultrabasic rocks have a variable Nb/Ta ratio (4.87–19.56), with an average of 12.94, while Luku alkali syenite has a Nb/Ta ratio of 14.27–18.73, with an average of 16.41, showing a significant difference. The Luku alkali syenite, compared with the coeval Hongge basic-ultrabasic rock and basalt, had an $^{87}Sr/^{86}Sr$ much higher than that of coeval basalts in the area (0.7049–0.7084; Xiao et al., 2003) and a $^{143}Nd/^{144}Nd$ much lower than that of basic-ultrabasic rocks (0.512522–0.512610; Xiao et al., 2003). Thus, the obvious difference in trace element characteristics between the Luku alkali syenite and the Hongge basic-ultrabasic rocks, cannot support a direct inheritance relationship between them.

Generally, if syenite formed after low pressure fractional crystallization of basaltic magma, the source rock would undergo segregation of plagioclase, syenite only showing weak negative Eu anomalies (Deng et al., 2004). On the other hand, experimental petrology and phase equilibrium research indicates that syenite magma also forms after partial melting. Under P = 1.5–1.7 GPa (near the base of the continental crust), the syenite often shows distinct negative Eu anomalies, because plagioclase was still present in the melt system. If the depth of the partial melt deepens so that the pressure exceeds 1.7 GPa, the solid phase line has no plagioclase, hence the syenite magma formed does not show negative Eu anomalies (Deng et al., 2004). Luo (2011) once performed modeling and calculation of partial melting of Indosinian Cida alkali rocks in the Panxi area using REE and discovered that pyroxene syenite can be formed when pyroxenitic cumulate rock is present in low degree partial melting (5%). In this study, the Luku alkali syenite showed obvious Eu negative anomalies (δEu = 0.73–0.80), similar to the coeval Cida alkali syenite. So it can be inferred that the Luku alkali syenite formed through the partial melting of source rocks at 55–60 km depth, with a low degree of

partial melting, or having plagioclase, apatite, rutile and sphene residuals, which agrees with characteristics of minor plagioclase and no apatite, rutile or sphene being present in the resulting alkali syenite.

In summary, the mantle plume origin of the mafic-supermafic rock from the Panxi area has been widely accepted (Munteanu et al., 2013), the mafic-supermafic rocks being produced by low degrees of melting of an enriched mantle source with EM2 characteristics (Zhou, 2005). The E'meishan basalt is the product of the interaction between the E'meishan mantle plume and the lithosphere (Xiao et al., 2003). The Luku alkali syenite, formed in the intraplate continental extension environment at the western margin of the Yangtze platform and showing crust-mantle derived characteristics, is closely associated with the contemporaneous and symbiotic layered basic-ultrabasic rocks in genesis, but not with an inheritance relationship between them. Basically, partial melting is a significant process for intraplate magma. Thus, we infer that thermal interactions occurred between the alkali syenite and the layered basic-ultrabasic rocks. The Luku alkali syenite was formed by the partial melting of crust-mantle granulite, forced by underplating of an uprising mantle plume of basic magma (Fig. 12).

5.4 Magma evolution and implications for mineralization

It has been noted that there are several kinds of alkaline rocks in the Luku alkali district, such as alkaline syenite, alkaline syenite pegmatite, alkaline albitite and alkaline granite. In terms of quantity, there are 86 alkaline syenite pegmatite veins, followed by 59 alkaline syenite veins and 17 alkaline albitite veins. In ore-bearing terms, alkaline albitite is the best, followed by alkaline syenite pegmatite, alkaline syenite having no industrial orebody. The Luku alkaline syenite intrusion yielded a zircon U-Pb age of 264.5 ± 1.6 Ma in this study, 6 Ma earlier than the ore-bearing alkaline rocks (258 Ma), such as alkaline albitite and alkaline syenite pegmatite (Wang et al., 2013). The ore-bearing alkaline rocks are often located in the outer contact zone of alkaline syenite intrusions. Combined with the analytical data of ore-bearing rock studied by Wang et al. (2015), the ore-bearing rocks have higher Na_2O contents than Nb-Ta-poor alkaline syenite. There are positive correlations of Na_2O, Nb and Ta for the rocks of the Nb-Ta-mineralized and Nb-Ta-poor syenitic dikes, which indicate that the enrichment of Nb and Ta in the Nb-Ta-mineralized syenitic dikes is likely related to the increase of Na. Given that the large amounts of fine-grained albite crystals in the Nb-Ta-mineralized syenitic dikes formed due to albitization, the enrichment of Nb and Ta is likely related to the late-stage fluid-rock interaction in the highly evolved magma. Based on the mineral calculations, Luku alkali syenite contains quartz, potassium feldspar and albite, but the ore-bearing rock mainly contains albite and less quartz, indicating that the magma is evolving towards the albite. It could be considered that the albitization of the Nb-Ta-mineralized syenitic dikes may have been caused by the autometasomatism in a transitional, magmatic-hydrothermal stage. So the genesis of the deposit belongs to the albite pegmatite deposit, relating it to the alkaline syenite.

Trace element concentration can provide simple and effective information for degree of magma fractionation. The basic principle is to select major and trace element pairs with similar crystal chemical properties (trace element pairs, i.e., REE) (Zhao, 2016). Zr and Hf are typical lithophilic elements, with very similar crystal chemical properties (such as ion radius and charge). They are usually concentrated in late stages of magmatism and typically enriched in pyroxene syenite (Kogarko, 2016). Due to the fractionation of alkaline pyroxene during alkaline magma evolution and fractionation, Zr/Hf increased accordingly (Kogarko, 2016). The Luku alkaline syenite had Zr concentrations of 49.2–79.4 ppm, Hf concentrations of 2.40–2.92 ppm and Zr/Hf ratio of 20.50–29.30 with an average of 26.36, which is much lower than that of alkali rocks of other typical REE deposits, such as the Ilímaussaq complex (Michael and Gregor, 2001) and the Lovozero lujavrite (Kramm and Kogarko, 1994). This further indicates that the magma source of the Luku alkali syenite had experienced a low degree of evolution and fractionation.

Long-term and complete fractionation and evolution of alkaline magma are the main factors controlling the crystallization of REE minerals and the REE mineralization of agpaitic alkaline intrusions (Kogarko, 2016). Thus, magma fractionation and the evolutionary

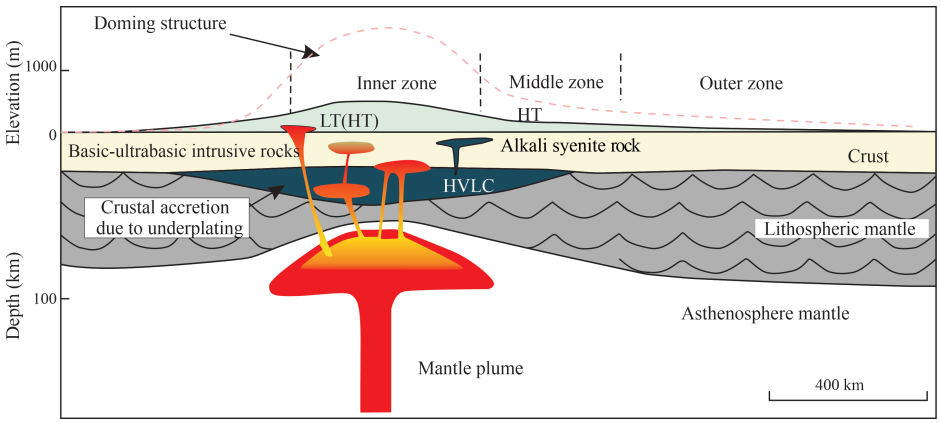

Fig. 12. A possible model for the formation of the Luku alkali syenite (after Zhang et al., 2019).
HVLC–high velocity lower crust; HT–high-Ti basalt; LT–low-Ti basalt.

degree of the Luku alkali syenite possibly determined the reason for the poor REE mineralization.

6 Conclusions

(1) The Luku alkali syenite yields a zircon U-Pb LA-ICP-MS age of 264.5 ± 1.6 Ma, concordant with the age (258 ± 4.1 Ma) of the Hongge layered basic-ultrabasic intrusive rock (Li et al., 2017) and the end time (251.0 ± 1.0 Ma) of the E'meishan basalt eruption (Zhu et al., 2011), within the margin of error. They are products of the same magmatism.

(2) Zircons from the Luku alkali syenite display intense positive Ce anomalies and negative Eu anomalies. The rock has a $^{176}Hf/^{177}Hf$ ranging from 0.282391 to 0.282574, averaging 0.282465, as well as $\varepsilon_{Hf}(t)$ ranging from −7.99 to −1.83, averaging −5.33 (<0). The rock mainly falls in the lower crust source area in the $\varepsilon_{Hf}(t)$-age plot (Fig. 11), indicating that it was sourced from ancient crust.

(3) The Luku alkali syenite, E'meishan basalt and Indosinian basic-ultrabasic intrusive rocks in the Panxi area are closely physically associated; when considered in conjunction with the partial melting model of the most common basaltic source of Na-rich magmatic origin, it can be inferred that the Luku alkali syenite was formed by the partial melting of crust-mantle granulite, forced by underplating of a mantle plume of basic magma.

(4) The main reason for the poor REE mineralization of the Luku alkali syenite may be related to the low degree of magma differentiation.

Acknowledgments

This work was supported by the China Geological Survey (Grant Nos. DD20189501 and DD20190446). We thank Dr. Hou Kejun for LA-ICP-MS zircon U-Pb dating.

Manuscript received Oct. 31, 2020
accepted Mar. 17, 2021
associate EIC: FANG Xiang
edited by Jeffery J. LISTON and GUO Xianqing

References

Andersen, T., 2002. Correction of common lead in U-Pb analyses that do not report ^{204}Pb. Chemical Geology, 192(1–2): 59–79.

Andrea, M., Festus, T.A., Renaud, M., Sara, C., and Jean, N., 2015. Deep to shallow crustal differentiation of within-plate alkaline magmatism at Mt. Bambouto volcano, Cameroon line. Lithos, 220–223: 272–288.

Astis, G.D., Peccerillo, A., and Kempton, P., 2000. Transition from calc-alkaline to potassium-rich magmatism in subduction environments: Geochemical and Sr, Nd, Pb isotopic constraints from the island of volcano (Aeolian arc). Contributions to Mineralogy and Petrology, 139(6): 684–703.

Belousova, E.A., Griffin, W.L., and Pearson, N.J., 1998. Trace element composition and cathodoluminescence properties of southern African kimberlitic zircons. Mineralogical Magazine, 62(3): 355–366.

Chen, J.F., and Jahn, B.M., 1998. Crustal evolution of southeastern China: Nd and Sr isotopic evidence. Tectonophysics, 284(1–2): 101–133.

Dai, L.Q., Zhao, Z.F., Zheng, Y.F., Li, Q.L., Yang, Y.H., and Dai, M.N., 2011. Zircon Hf-O isotope evidence for crust-mantle interaction during continental deep subduction. Earth and Planetary Science Letters, 308: 229–244.

Daniel, M., and David, I.G., 2019. Potassic igneous rocks and associated gold-copper mineralization. Switzerland: Springer International Publishing AG, 1–398.

Deng, J.F., Luo, Z.H., Su, S.G., Mo, X.X., Yu, B.S., and Lai, X.Y., 2004. Rock genesis, tectonic setting and mineralization. Beijing: Geological Publishing House, 60–61 (in Chinese).

Elhlou, S., Belousova, E., Griffin, W.L., Pearson, N.J., and O'Reilly, S.Y., 2006. Trace element and isotopic composition of GJ-red zircon standard by laser ablation. Geochimica et Cosmochimica Acta, 70(18) suppl: A158.

Foley, S., 1992. Vein-plus-wall-rock melting mechanisms in the lithosphere and the origin of potassic alkaline magmas. Lithos, 28: 435–453.

Frost, B.R., and Frost, C.D., 2008. A geochemical classification for feldspathic igneous rocks. Journal of Petrology, 49(11): 1955–1969.

Gomes, C.B., Ruberti, E., Comin, C.P., and Azzone, R.G., 2011. Alkaline magmatism in the Ponta Grossa Arch, SE Brazil: A review. Journal of South American Earth Sciences, 32: 152–168.

Goton, M.P., and Schandl, E.S., 2000. From continents to island arcs: A geochemical index of tectonic setting for arc-related and within-plate felsic to intermediate volcanic rocks. The Canadian Mineralogist, 38(5): 1065–1073.

Green, T.H., 1995. Significance of Nb/Ta as an indicator of geochemical processes in the crust-mantle system. Chemical Geology, 120: 347–359.

Griffin, W.L., Belousova, E.A., and Shee, S.R., 2004. Archean crustal evolution in the northern Yilarn craton: U-Pb and Hf-isotope evidence from detrital zircons. Precambrian Research, 131(3–4): 231–282.

Griffin, W.L., Wang, X., Jackson, S.E., Pearson, N.J., O'Reilly, S.Y., Xu, X.S., and Zhou, X.M., 2002. Zircon chemistry and magma mixing, SE China: In-situ analysis of Hf isotopes, Tonglu and Pingtan igneous complexes. Lithos, 61: 273–269.

He, X.X., Zhu, X.K., Yang, C., and Tang, S.H., 2005. High-precision analysis of Pb isotope ratios using MC-ICP-MS. Acta Geoscientica Sinica, 26(Supp), 19–22 (in Chinese with English abstract).

Helena, C.B.M., Pedro, P.S., and Joana, A., 2014. Zircon crystal morphology and internal structures as a tool for constraining magma sources: Examples from northern Portugal Variscan biotite-rich granite plutons. Comptes Rendus Geoscience, 346: 233–243.

Hoskin, P.W.O., Kinny, P.D., Wyborn, D., and Chappell, B.W., 2000. Identifying accessory mineral saturation during differentiation in granitoid magmas: An integrated approach. Journal of Petrology, 41(9): 1365–1396.

Hou, K.J., Li, Y.H., Zou, T.R., Qu, X.M., Shi, Y.R., and Xie, G.Q., 2007. Laser ablation MC-ICP-MS technique for Hf isotope microanalysis of zircon and its geological applications. Acta Petrologica Sinica, 23(10): 2595–2604 (in Chinese with English abstract).

Hou, K.J., Li, Y.H., and Tian, Y.R., 2009. In situ U-Pb zircon dating using laser ablation-multi ion counting-ICP-MS. Mineral Deposit, 28(4): 481–492 (in Chinese with English abstract).

Hou, Z.Q., Tian, S.H., Xie, Y.L., Yang, Z.S., Yuan, Z X., Yin, S.P., Yi, L.S., Fei, H.C., Zou, T.R., Bai, G., and Li, X.Y., 2009 The Himalayan Mianning–Dechang REE belt associated with carbonatite-alkaline complexes, eastern Indo-Asian collision zone, SW China. Ore Geology Reviews, 36: 65–89.

Hu, S.F., Zhong, H., Liu, B.G., and Zhou, X.H., 2001. Geochemistry of the Hongge layered intrusion in the Panxi area. Geochimica, 30(2): 131–139 (in Chinese with English abstract).

Kaygusuz, A., Aslan, Z., Aydinçakir, E., Yücel, C., Gücer, M.A., and Şen, C., 2018. Geochemical and Sr-Nd-Pb isotope characteristics of the Miocene to Pliocene volcanic rocks from the Kandilli (Erzurum) area, eastern Anatolia (Turkey): Implications for magma evolution in extension-related origin. Lithos, 299: 332–351.

Kieffer, B., Arndt, N., and Lapierre, H., 2004. Flood and shield basalts from Ethiopia: Magmas from the African superswell. Journal of Petrology, 45(4): 793–834.

Kinny, P.D., and Maas, R., 2003. Lu-Hf and Sm-Nd isotope systems in zircon. Reviews in Mineralogy and Geochemistry, 53(1): 327–341.

Kogarko, L.N., 2016. Geochemistry of fractionation of coherent elements (Zr and Hf) during the profound differentiation of peralkaline magmatic systems: A case study of the Lovozero complex. Geochemistry International, 54(1): 1–6.

Kramm, U., and Kogarko, L.N., 1994. Nd and Sr isotope signatures of the Khibina and Lovozero agpaitic centres, Kola Alkaline Province, Russia. Lithos, 32: 225–242.

Lei, W.Y., Shi, G.H., and Liu, Y.X., 2013. Research progress on trace element characteristics of origins. Earth Science Frontiers, 20(4): 273–284 (in Chinese with English abstract).

Li, B., and Jiang, S.Y., 2014. Geochronology and geochemistry of Cretaceous Nanshanping alkaline rocks from the Zijinshan district in Fujian Province, South China: Implications for crust -mantle interaction and lithospheric extension. Journal of Asian Earth Sciences, 93: 253–274.

Li, H., Koichiro, W., and Kotaro, Y., 2014. Zircon morphology, geochronology and trace element geochemistry of the granites from the Huangshaping polymetallic deposit, South China: Implications for the magmatic evolution and mineralization processes. Ore Geology Reviews, 60: 14–35.

Li, H.Q., Wang, D.H., Zhang, L.G., Ren, H.T., Wang, X.D., Jia, X.H., and Yang, W.Q., 2017. SHRIMP U-Pb and Sm-Nd dating of the gabbro and syenite from the Hongge ore district in western Panzhihua and its geological significance. Geological Bulletin of China, 36(5): 698–705 (in Chinese with English abstract).

Li, X.H., Liang, X.R., Sun, M., Liu, Y., and Tu, X.G., 2000. Geochronology and geochemistry of single-grain zircon: Simultaneous in-situ analysis of U-Pb age and trace elements by LAM-ICP-MS. European Journal of Mineralogy, 12(5): 1015–1024.

Lin, Q.C., Xia, B., and Zhang, Y.Q., 2006. Zircon SHRIMP U-Pb dating of the Cida alkali complex in the Dechang area, southern Sichuan, China. Geological Bulletin of China, 25(3): 398–401 (in Chinese with English abstract).

Liu, F., Zhang, C.J., Wang, Y.L., and Shi, Z.M., 2005. Geochemical characteristics of Th, Ta and Hf in mafic-alkaline rock series in the Panzhihua area. Computing Techniques for Geophysical and Geochemical Exploration, 27 (1): 43–47 (in Chinese with English abstract).

Liu, Y.S., Hu, Z.C., Gao, S., Gunther, D., Xu, J., Gao, C., and Chen, H., 2008. In situ analysis of major and trace elements of anhydrous minerals by LA-ICP-MS without applying an internal standard. Chemical Geology, 257(1–2): 34–43.

Lu, Y.F., 2004. Geokit—A geochemical toolkit for Microsoft Excel. Geochimica, 33(5): 459–564 (in Chinese with English abstract).

Ludwig, K.R., 2003. User's Manual for Isoplot/Ex Version 3.00: A Geochronological Toolkit for Microsoft Excel. Berkeley: Berkeley Geochronology Center Special Publication, 4(2): 1–70.

Luo, W.J., Zhang, Z.C., Hou, T., and Wang, M., 2011. Geochronology and geochemistry of the Cida complex in the Panxi district: Constraints on the duration of the Emeishan mantle plume. Acta Petrologica Sinica, 27(10): 2947–2962 (in Chinese with English abstract).

Luo, Z.Y., Xu, Y.G., He, B., Shi, Y.R., and Huang, X.L., 2006. Discussion of the genetic relationship between the Maomaogou nepheline syenite and the Emeishan large igneous province in the Panxi area: Chronology and geochemical evidence. Science Bulletin, 51(15): 1802–1810 (in Chinese).

Miao, Y.K., Ren, Z.D., and Chen, X.Y., 1986. Tectonic environment and tectonic development of the Panxi rift in Sichuan. Earth Science-Journal of Wuhan College of Geology, 11(6): 631–637 (in Chinese with English abstract).

Michael, M., and Gregor, M., 2001. Fractionation and assimilation processes in the alkaline augite syenite unit of the Ilimaussaq intrusion, South Greenland, as deduced from phase equilibria. Journal of Petrology, 42(10): 1947–1969.

Middlemost, E.A.K., 1975. The basalt clan. Earth Science Reviews, 11: 337–364.

Muller, D., Franz, L., Herzig, P.M., and Hunt, S., 2001. Potassic igneous rocks from the vicinity of epithermal gold mineralization, Lihir Island. Papua New Guinea. Lithos, 57: 163–186.

Munteanu, M., Yao, Y., Cioacă, M., Chunnett, G., and Luo, Y.N., 2011. A reconnaissance study on selected intrusive bodies south of Panzhihua, Sichuan Province, South-West China: Petrogenetic and metallogenetic significance. Romanian Journal of Earth Sciences, 85(1): 19–34.

Munteanu, M., Yao, Y., Wilson, A.H., Chunnett, G., Luo, Y.N., and He, H., 2013. Panxi region (South-West China): Tectonics, magmatism and metallogenesis. A review. Tectonophysics, 608: 51–71.

Nardi, L.V.S., Formoso, M.L.L., Jarvis, K., Oliveira, L., Bastos, N.A.C., and Fontana, E., 2012. REE, Y, Nb, U, and Th contents and tetrad effect in zircon from a magmatic-hydrothermal F-rich system of Sn-rare metal-cryolite mineralized granites in the Pitinga Mine, Amazonia, Brazil. Journal of South American Earth Sciences, 33(1): 34–42.

Ni, S.J., Teng, Y.G., Zhang, C.J., and Wu, X.Y., 1999. Review on the geochemical tracing of mineralizing fluid. Advances in Earth Sciences, 14(4): 346–352 (in Chinese with English abstract).

Rudnick, R.L., and Gao, S., 2003. Composition of continental crust. Treatise on Geochemistry, 3: 1–65.

Shellnutt, J.G., and Zhou, M.F., 2008. Permian, rifting related fayalite syenite in the Panxi region, SW China. Lithos, 101: 54–73.

Sokól, K., Halama, R., Meliksetian, K., and Savov, I.P., 2018. Alkaline magmas in zones of continental convergence: The Tezhsar volcano-intrusive ring complex, Armenia. Lithos, 320 –321: 172–191.

Song, B., Zhang, Y.H., Wan, Y.H., and Jian, P., 2002. Mount making and procedure for SHRIMP dating. Geological Review, 48(Supp): 26–30 (in Chinese with English abstract).

Sun, S.S., and McDonough, W.F., 1989. Chemical and isotopic systematics of oceanic basalts: Implications for mantle composition and processes. In: Saunders, A.D., and Norry, M.J. (eds.), Magmatism in the Ocean Basins. Geological Society London Special Publications, 42: 313–345.

Taylor, S.R., and McLennan, S.M., 1985. The continental crust: Its composition and evolution: an examination of the geochemical record preserved in sedimentary rocks. Oxford: Blackwell Oxford, 1–312.

Wang, F.L., Wang, C.Y., and Zhao, T.P., 2015. Boron isotopic constraints on the Nb and Ta mineralization of the syenitic dikes in the ~260 Ma Emeishan large igneous province (SW China). Ore Geology Reviews, 65: 1110–1126.

Wang, F.L., Zhao, T.P., Chen, W., and Wang, Y., 2013. Zircon U-Pb ages and Lu-Hf isotopic compositions of the Nb-Ta-Zr bearing syenitic dikes in the Emeishan large igneous province. Acta Petrologica Sinica, 29(10): 3519–3532 (in Chinese with English abstract).

Weyer, S., Munker, C., Rehkamper, M., and Mezger, K.,2002. Determination of ultra-low Nb, Ta, Zr and Hf concentrations and the chondritic Zr/Hf and Nb/Ta ratios by isotope dilution analyses with multiple collector ICP-MS. Chemical Geology, 187: 295–313.

Wright, J.B., 1969. A simple alkalinity ratio and its application to questions of non-orogenic granite genesis. Geological Magazine, 106(4): 1102–1108.

Wu, Y.B., Chen, D.G., Zheng, Y.F., Xia, Q.K., and Tu, X.L., 2004. Trace element geochemistry of zircons in migmatitic genesis at Manshuihe, North Dabieshan and its geological implications. Acta Petrologica Sinica, 20(5): 1141–1150 (in Chinese with English abstract).

Xiao, L., He, Q., Pirajno, F., Ni, P.Z., Du, J X., and Wei, Q.R., 2008. Possible correlation between a mantle plume and the evolution of Paleo-Tethys Jinshajiang Ocean: Evidence from a volcanic rifted margin in the Xiaru-Tuoding area, Yunnan, SW China. Lithos, 100: 112–126.

Xiao, L., Xu, Y.G., and He, B., 2003. Emei mantle plume-subcontinental lithosphere interaction: Sr-Nd and O isotopic evidence from low-Ti and high-Ti basalts. Geological Journal of China Universities, 9(2): 207–217 (in Chinese with English

abstract).
Xiao, L., Xu, Y.G., Mei, H.J., Zheng, Y.F., He, B., and Pirajno, F., 2004. Distinct mantle sources of low-Ti and high-Ti basalts from the western Emeishan large igneous province, SW China: Implications for plume-lithosphere interaction. Earth and Planetary Science Letters, 228(3–4): 525–546.
Xu, D., Wang, R., Wang, W.G., Ge, Q., Zhang, W.L., and Chen, L., 2019. Tracing the source of Pb using stable Pb isotope ratios in sediments of the eastern Beibu Gulf, South China Sea. Marine Pollution Bulletin, 141:127–136.
Xu, Y.G., and He, B., 2007 Thick and high velocity crust in Emeishan large igneous province, SW China: Evidence for crustal growth by magmatic underplating or intraplating. In: Foulger, G., and Burdy, D. (eds.), The origins of Melting Anomalies: Plates, Plumes, and Planetary Processes. Geological Society of America Special Paper, 430: 841–858.
Xu, Y.G., Chung, S.L., Jahn, B.M., and Wu, G.Y., 2001. Petrologic and geochemical constraints on the petrogenesis of Permian–Triassic Emeishan flood basalts in southwestern China. Lithos, 58(3–4): 145–168.
Xu, Z.Q., Li, H.Q., Hou, L.W., Fu, X.F., Chen, W., Zeng, L.S., Cai, Z.H., and Chen, F.Y., 2007. Uplift of the Longmen-Jinping orogenic belt along the eastern margin of the Qinghai-Tibet plateau: Large-scale detachment faulting and extrusion mechanisms. Geological Bulletin of China, 26(10): 1262–1276 (in Chinese with English abstract).
Zhang, B.R., and Fu, J.M., 2005. Advances in Geochemistry. Beijing: Chemical Industry Press, 1–437 (in Chinese).
Zhang, H.F., Zhong, Z.Q., Gao, S., Zhang, B., Zhang, L., Hu, S.Y., and Hou, Q.Y., 2004. Pb and Nd isotopic composition of the Jigongshan granite: Constraints on crustal structure of Tongbaishan in the middle part of the Qinling-Tongbai-Dabie orogenic belt, central China. Lithos, 73: 215–227.
Zhang, M., Liu, X.F., Zhao, F.F., Deng, B.P., Chu, Y.T., Dong, Y., and Huang, Y.P., 2014. Characteristics, genesis and metallogenic significance of Machangqing adakite porphyry rich in alkali from Western Yunnan, China. Journal of Chengdu University of Technology (Science Technology Edition), 41(2): 217–226 (in Chinese with English abstract).
Zhang, Y.X., Luo, Y.N., and Yang, C.X., 1988. Panxi Rift Valley. Beijing: Geological Publishing House, 1–100.
Zhang, Z.H., Qin, J.F., Lai, S.C., Long, X.P., Ju, Y.J., Wang, X.Y., Zhu, Y., and Zhang, F.Y., 2019. Origin of Late Permian syenite and gabbro from the Panxi rift, SW China: The fractionation process of mafic magma in the inner zone of the Emeishan mantle plume. Lithos, 346–347: 1–12.
Zhao, Z.H., 2016. Trace Element Geochemistry. Beijing: Science Press, 115–393 (in Chinese).
Zhong, H., Hu, R.Z., Zhu, W.G., and Liu, B.G., 2007a. Genesis and mineralization of layered intrusions. Earth Science Frontiers, 14(2): 159–172 (in Chinese with English abstract).
Zhong, H., Zhu, W.G., Chu, Z.Y., He, D.F., and Song, X.Y., 2007b. SHRIMP U-Pb zircon geochronology, geochemistry, and Nd-Sr isotopic study of contrasting granites in the Emeishan large igneous province, SW China. Chemical Geology, 236: 112–133.
Zhou, J.Y., Tan, H.Q., Gong, D.X., Zhu, Z.M., and Luo, L.P., 2018. Zircon U-Pb age, trace element, and Hf isotopic compositions of Nordmarkite in the Lizhuang rare earth element deposit in the western margin of the Yangtze Block. Acta Geologica Sinica (English Edition), 92(1): 225–240.
Zhou, L.D., Zhao, Z.H., and Zhou, G.F., 1996. Isotopic chronology of some alkaline rock bodies in China. Geochimica, 25(2): 164–171 (in Chinese with English abstract).
Zhou, M.F., 2005. Origin of layered gabbroic intrusions and their giant Fe-Ti-V oxide deposits in the Panxi district, Sichuan Province SW China. Acta Petrologica et Mineralogica, 24(5): 381–384 (in Chinese with English abstract).
Zhou, M.F., Chen, W.T., Wang, C.Y., and Prevec, S.A., 2013. Two stages of immiscible liquid separation in the formation of the Panzhihua-type Fe-Ti-V oxide deposits, SW China. Geoscience Frontiers, 4: 481–502.
Zhou, M.F., Yan, D.P., Kennedy, A.K, Li, Y.Q., and Ding, J., 2002. SHRIMP U-Pb zircon geochronological and geochemical evidence for Neoproterozoic arc-magmatism along the western margin of the Yangtze Block, South China. Earth and Planetary Science Letters, 196(1–2): 51–67.
Zhu, J., Zhang, Z. C., Hou, T., and Kang, J.L., 2011. LA-ICP-MS zircon U-Pb geochronology of the tuffs on the uppermost of the Emeishan basalt succession in Panxian County, Guizhou Province: Constraints on the genetic link between Emeishan large igneous province and the mass extinction. Acta Petrologica Sinica, 27(9): 2743–2751 (in Chinese with English abstract).
Zindler, A., and Hart, S.R., 1986. Chemical geodynamics. Annual Review of Earth and Planetary Sciences, 14: 493–571.

About the first and corresponding author

ZHOU Jiayun, male, born in 1973 in Dayi County, Sichuan Province; doctor; professorate senior engineer of the Institute of Multipurpose Utilization of Mineral Resources, Chinese Academy of Geological Sciences. He is currently interested in deposit geochemistry. E-mail: zhszjy@aliyun. com; phone: 028-85592028, 13608211820.